Variable evapotranspirative water losses from lowland agricultural and native shrubland ecosystems in the eastern Great Basin of Nevada, USA

Arnone JA III*, Jasoni RL, Larsen JD, Fenstermaker LF, Wohlfahrt G, Kratt CB, Lyles BF, Healey J, Young MH, Thomas JM

* John A. Arnone III, Corresponding Author
  Desert Research Institute
  2215 Raggio Parkway
  Reno, NV 89511, USA

  Tel. (775) 673-7445
  Fax. (775) 673-7485
  jarnone@dri.edu

6 August 2008

Abstract (Executive Summary)

Development of new ground water resources in rural lands surrounding urban areas of the arid western United States has been identified as a key to maintaining the economic viability of this region. The extent and rate at which ground water can be sustainably extracted, while avoiding or minimizing environmental impacts, depends to a large degree on how much of the existing resource escapes back to the atmosphere via the process of evapotranspiration (ET). ET is the sum of water that evaporates (E) from soil surfaces and is transpired (T) from surfaces of leaves as plants pull water through their roots and stems from the unsaturated soil in the vadose zone or from ground water in the saturated substrate.

The primary objective of the study presented here was to quantify ET from four lowland basin sites in Spring Valley, Nevada, for one year (April 2007 to April 2008). All sites represented a diversity of typical lowland sites in the valley: three shrubland sites and one managed perennial grassland site. A secondary objective was to use ET rates measured at these four sites, in combination with vegetation indices (Normalized Difference Vegetation Index: NDVI, and Enhance Vegetation Index: EVI) calculated from Landsat TM 5 satellite data for the growing season, to extrapolate ET rates to the entire valley. To accomplish these objectives, the study also addressed several necessary preliminary objectives. These included: (a) a comparison of estimates of ET derived using eddy covariance (EC, a method that relies on the sensitive measurement of vertical wind speed and water vapor density), with simultaneous direct water vapor flux measurements of ET using a static chamber to assess confidence in ET estimates calculated from the continuous EC method; (b) development of empirical relationships

between ET measurements from EC tower footprint areas with satellite-derived vegetation indices on several dates at each site, to determine whether these indices could be used reliably as tools to extrapolate to large land areas; (c) evaluation of a method that uses changes in ground water level (logging well hydrographs) from wells screened across the water table at each site as another means for estimating local-scale water losses from phreatophytic plant transpiration; and (d) use of best regression equations between NDVI, or EVI, and measured ET at each site developed in (b), together with vegetation indices of the entire lowland basin (valley) phreatophytic zone, to estimate whole-valley ET losses for the study year.

One EC tower was installed at each of the four sites in April 2007. Towers included all instrumentation and dataloggers necessary to continuously quantify latent heat flux for subsequent calculations of water vapor flux and ET. Water table level data obtained from a ground water observation well installed adjacent to each EC tower were also recorded. All raw 10 Hz EC data were analyzed using a full suite of well-established methods. On two (or three) dates ET was measured within the local footprint of each EC tower using a large static chamber. Five to fifteen representative 12.3 m^2 plots were established for the chamber measurements, which were monitored during a 36-hour period. The resulting ET rates were compared to ET rates calculated from EC data collected during that same period to constrain ET estimates derived from EC calculations. Landsat TM image data used for developing empirical relationships with ET were acquired on nine cloud-free dates during the growing season.

Annual ET calculated from continuous EC measurements varied widely across all four sites with the grassland site (659 mm year^{-1}) causing most of this variability. ET

from the shrubland sites clustered at much lower values: 172 (Spring Valley EC site 7:

SV7), 238 (site SV6) and 260 (site SV5) mm year^{-1}. High vegetation indices

corresponded to dense grass cover at the grassland site, and lower vegetation indices

corresponded to relative sparse cover at the shrub sites. Vegetation indices accounted for

much of the variability observed in annual ET measured with EC (r^2: 0.93 to 0.99).

However, correlations observed between vegetation indices and ET on individual dates

and individual sites were not strong and indicated that vegetation indices could not be

used reliably to estimate seasonal changes in ET for a site or for the entire valley (based

on this one year of data). Strongest correlations between vegetation indices and ET were

observed at the annual time scale and across all sites. These strong correlations enhanced

confidence in using either mean growing season NDVI or EVI to extrapolate from site-

level annual ET measured with EC to basin-wide annual ET. Extrapolated annual basin-

wide ET estimates derived from calculations using NDVI were 6 to 10% lower than

estimates derived from calculations using EVI. Basin-wide ET calculated using a single

regression equation (annual ET on NDVI, or on EVI) across all four sites also differed

from basin-wide ET calculated using separate equations for shrub and grassland sites.

The decision to assess differences between single and double equations was based on the

frequency distribution of NDVI and EVI values that showed greater than 80% of all data

within the basin falling within the range observed at the shrub sites, and less than 10% of

the data falling above that. Whole-basin ET estimated using mean growing season NDVI

and annual ET ranged from 222,871 acre feet year^{-1} (single equation) to 204,628 acre feet

year^{-1} (two equations).

Intensive comparison of ET rates measured with EC and the large static chamber dome with data pooled across all four sites on multiple chamber sampling dates during the study year indicated that dome-adjusted annual EC ET were 16% lower than non-adjusted EC ET fluxes. Within-site comparisons of ET estimates calculated using the two methods indicated that dome-adjusted annual EC ET were 29% lower than non-adjusted EC ET fluxes. These adjustments corresponded to a range in whole-basin ET estimates of 145,286 to 158,238 acre feet year^{-1} using NDVI, and 159,709 to 171,093 acre feet year^{-1} using EVI.

Analysis of data from ground water monitoring wells provided some indications that daily and seasonal changes in water levels may hold some promise for estimating ET on sites known to be dominated by phreatophytes (e.g. greasewood, *Sarcobatus vermiculatus*) for short periods when plants are actively transpiring. However, in the absence of other data for this project (e.g. substrate porosity, hydraulic conductivity, pumping records), ground water level data collected during the study year were of limited utility for quantitatively estimating phreatophytic ET. The supplementary data listed above are needed to evaluate the potential for using fluctuations in ground water levels to quantify phreatophytic ET from very large land areas (e.g. Loheide *et al.* 2005).

Together, results from this one-year study provide some new quantitative estimates of site-specific and basin-wide ET that should help improve the accuracy of estimating ET from Spring Valley. Because our study focused on the measurement of total ET, where the water source originates in the vadose and saturated zones, we were unable to quantitatively separate the magnitude of both sources. To better estimate the phreatophytic contribution to total ET, which is more reflective of actual ground water

use by plants/vegetation, a more comprehensive analysis that includes isotopic examination (e.g. ^{18}O in soil, plant and ground water) would be extremely powerful. Finally, the sizeable range of ET estimates presented for the single year of our study suggest that using multiple measurement and extrapolation methods, along with inclusion of some additional techniques, would significantly enhance future estimates of total and phreatophytic ET.

List of Abbreviations

1) Automatic gain control (AGC)

2) Eddy covariance (EC)

3) Enhanced Vegetation Index (EVI)

4) Evapotranspiration (ET)

5) Normalized Difference Vegetation Index (NDVI)

6) Photon flux density (PFD)

7) Photosynthetically active radiation (PAR)

8) Polyvinyl chloride (PVC)

9) Region of interest (ROI)

10) Spring Valley eddy covariance tower locations 4, 5, 6, 7 (SV4, SV5, SV6, SV7)

11) Webb, Pearman, Leuning density correction (WPL)

REPORT CONTENTS

Introduction

Demand for water in arid regions of the world continues to rise as populations in urban areas within these arid areas increase. In the arid southwestern United States, urban population and economic growth in cities such as Los Angeles, Phoenix, Albuquerque and Las Vegas—and in large agricultural areas of western Texas, southern Arizona and southern California—have accelerated the demand for water (Naumburg et al. 2005, Hatton et al. 1998, Puigdefabregas & Mendizabal 1998, Le Maitre et al. 1999, Zhu et al. 2004) to a degree that has become increasingly more difficult to meet by traditional surface water sources (e.g. the Colorado River; Committee on the Scientific Basis of Colorado River Basin Water Management 2007). This increase in demand and decrease in surface water supply has necessitated the consideration of an increased use of ground water to meet this shortfall. While ground water aquifers have been tapped for agricultural irrigation in the southwestern U.S. for many years (e.g. Jury & Vaux 2007; Norwood 2000; Allen et al. 2008; Allen et al. 2005), the extent to which additional ground water pumping is effecting ground water levels, ground water sustainability, and the ecology of basin ecosystems are generally unknown and require a more quantitative understanding of basin ecosystem water budgets.

The amount of water "lost" from these ecosystems via evapotranspiration (ET) is critical to determining water budgets of arid ecosystems of the U.S. (Flerchinger et al. 1996; Nichols 1993; Nichols 1994). However, ET data are sparse and highly variable in the western U.S. (Nichols 1993). Calculating and predicting the sustainability of ground water supplies and potentially negative environmental responses of additional ground water removal is difficult without a broader and more diverse dataset. Perennial woody

shrub and agricultural plant communities that occur in the valley floors of the Great Basin ecosystem (mostly in Nevada, USA) may remove significant amounts of water from both the unsaturated soil zone (thought to consist mostly of precipitation water), as well as the saturated ground water zone (phreatophytic transpiration, see Meinzer 1927, Nichols 1993), via plant transpiration (i.e. T of ET). Despite the awareness of the need for quantitative ET flux data to construct accurate ecosystem water budgets (e.g. White 1932; Nichols 1993; Nichols 1994), relatively few quantitative empirical ET data are available from these regions, upon which water management decisions (especially pumping of ground water) can be based. Also, the quantitative methods used thus far to measure (or estimate) actual ET in the field, like eddy covariance (e.g. Baldocchi *et al.* 2001) and weighing lysimeters (Young *et al.* 1996), have not been sufficiently compared to other methods of measuring ecosystem ET like large static chambers (Arnone & Obrist 2003; Obrist *et al.* 2003) or small static chambers (Denmead *et al.* 1993; Dugas *et al.* 1997; Heijmans *et al.* 2004; Stannard *et al.* 2006; Prater & Delucia 2006). These quantitative comparisons can help mutually constrain estimates derived from both methods. Finally, developing relationships between ET rates and remotely sensed (satellite, low altitude color photos) and environmental data, from plot to footprint to basin scales have only recently been explored in detail (Devitt *et al.* 2008; Glenn *et al.* 2007; Groeneveld *et al.* 2007; Nagler *et al.* 2007), and their use by water managers would be enhanced if the relationships could be better quantified from local ET measurements to basin-scale ET estimates.

The objectives of this study were to: (1) quantify ET rates during a one-year period from four representative sites within the phreatophyte areas of Spring Valley, NV;

(2) compare eddy covariance (EC) derived estimates of ET, which are continuous and direct, with simultaneous static chamber measurements of ET, which are non-continuous and direct; (3) correlate ET measurements from EC tower footprint areas with satellite-derived vegetation indices to determine how well empirical relationships extrapolate ET to large land areas; (4) use changes in ground water level (logging well hydrographs) from wells screened across the water table at each site as another means for estimating local-scale phreatophytic ET losses (e.g. Robinson 1958; White 1932; Troxell 1936; Gatewood *et al.* 1950; Meyboom 1967; Tromble 1977; Gerla 1992; Rosenberry & Winter 1997; Lewis *et al.* 2002; Loheide *et al.* 2005); and (5) use regression equations developed in (3), and vegetation index images from entire lowland basin (valley) phreatophytic zone, to estimate whole-valley total annual ET loss.

Material and Methods

Study sites

Four sites were selected in Spring Valley in eastern Nevada, USA (39°10' N 114° 26' W), that were considered to be representative of common valley-bottom plant communities in the Great Basin (**Fig. 1**). Three sites were covered with native shrub communities, ranging from sparse (Spring Valley EC tower location 7: SV7) to dense cover (Spring Valley EC tower location 5: SV5 and Spring Valley EC tower location 6: SV6), and one site was covered by a cultivated grassland community (Spring Valley EC tower location 4: SV4) (**Table 1**). Percentage plant canopy cover immediately around the shrub-dominated tower sites, measured at approximately 100 m radius, consisted of homogeneous stands of greasewood (*Sarcobatus vermiculatus* L.) at SV7 (19% cover)
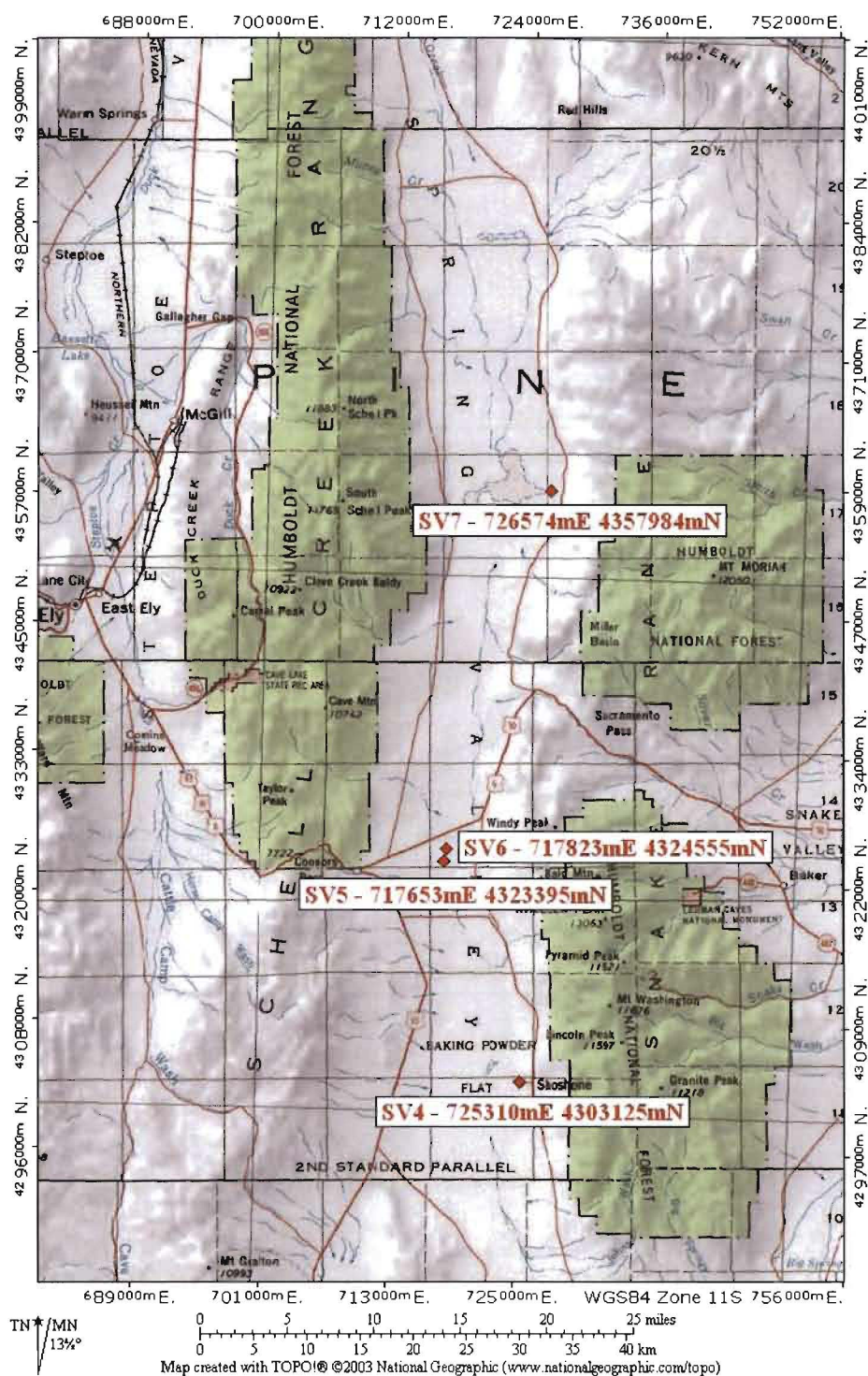
Figure 1. Topographic map (scale: 1:250,000; issue date: 2003) of Spring Valley in eastern Nevada, USA showing the location of the four study sites (SV4, SV5, SV6 and SV7) with their respective UTM (universal transverse mercator) coordinates (map datum: WGS84, Zone 11S).

Table 1. Study-year: average air temperature, air relative humidity--RH, air vapor pressure deficit--VPD, soil temperature; and total precipitation. Soil texture and depth to ground water table were measured during well contruction (May 2007). Vegetation cover was measured from a September 2004 1-m-resolution IKONOS image.

Characteristic		SV4	SV5	SV6	SV7
Air temperature (2 m, °C)		8.4	8.0	8.6	9.0
Air relative humidity (2 m, %)		58.3	57.0	55.1	52.1
Air VPD (2 m, kPa)		0.87	0.95	0.98	1.05
Soil temperature (-0.08 m, °C)		9.5	8.7	10.2	11.1
Precipitation (mm)		150	134	127	91
Vegetation cover (% land area in EC annual tower footprint)		84	42	31	13
Soil texture	0.0-0.6 m	Silt-loam	Silt-loam	Silt-loam	Silt-loam
	1.5-2.1 m	Clayey silt	Silt and gravel	Clay	Clay
	3.0-3.6 m	Sand and gravel	Silt and clay	Silt	Clay
	4.5-5.1 m	Silty clay and gravel	Silt, sand, and gravel	Sand and clay	Clay
	6.0-6.7 m	Silt and sand	Sand, clay, and gravel	Clay	Clay and silt
	7.6-8.2 m		Gravel and clay	Sand, clay, and gravel	Clay and silt
	9.1-9.7 m		Gravel and clay		Clay and silt
	10.6-11.2 m		Sand and gravel		
	11.5-12.1 m		Sand and gravel		
Ground water table depth (m)		2.50	7.70	5.39	5.07

and mixed stands of equal amounts of greasewood, sagebrush (*Artemisia tridentata*), and

rabbitbrush (*Chrysothamnus nauseosus*,) at sites SV5 (87% cover) and SV6 (76% cover).

The area immediately around the EC tower at site SV4 was dominated by pure grassland

communities. However, the percentages of plant cover within the area represented by

each EC tower (which was much larger than the 100-m radius) were smaller: 58% for

SV4, 14% for SV5, 21% for SV6, and 14% for SV7 (see method in Cablk & Kratt 2007).

Depth to ground water measured in open boreholes prior to well construction (May 2007)

for each of the sites were: 2.50 m for SV4, 7.70 m for SV5, 5.39 m for SV6, and 5.07 m

for SV7. Actual climate and soil data for the study period are shown in **Table 1**.

Eddy covariance instrumentation and calculations

In April 2007, EC and meteorological instrumentation were installed at each of

the four sites. The 3-m tall EC and meteorological towers were positioned downwind of

the dominant wind direction to capture ET fluxes of the dominant vegetation cover at

each site. The instruments installed on each EC tower consisted of a three-dimensional

sonic anemometer (CSAT3, Campbell Scientific Inc., Logan, Utah, USA) to measure the

three wind components, and an open-path infrared gas analyzer (IRGA) to measure H_2O

molar density (LI-7500, LI-COR Inc., Lincoln, Nebraska, USA). All sensors on each EC

tower were mounted 1 m above mean vegetation height on the south (predominant wind

direction) side of the tower. Weather and soil instruments at each site were mounted on

an adjacent 3 m tower and consisted of a shielded air temperature and humidity sensor

(2.0 meters above ground surface), wind vane anemometer (2.5 meters above ground

surface), net radiometer (1.8 meter above ground surface), photosynthetically active

radiation (PAR, 400-700 nm) sensor (2.5 meters above ground surface), tipping bucket

rain gauge (2.5 meters above ground surface), soil heat flux plates (8-cm soil depth), and

a soil temperature thermocouple (8-cm soil depth). Data from all instruments were

recorded with a data logger (CR5000, Campbell Scientific) at a frequency of 10 Hz (10

times per second) and stored on a compact flash card for post-processing. Data from each

logger were downloaded monthly when instruments were also checked and maintained.

Beginning on 20 April 2007, average ET for each half-hour period, including

sensible (H) and latent (LE) heat fluxes were measured using the EC method (Baldocchi

et al. 2001; Baldocchi 2003). Raw data (10 Hz) of the three wind components, the speed

of sound, and H_2O molar density were post-processed using the software *EdiRe*

(University of Edinburgh, UK). Eddy fluxes were calculated as the covariance between

turbulent fluctuations of the vertical wind speed and the water vapor density derived from

Reynolds (block) averaging of 30-minute blocks of data. The sonic anemometer's

coordinate system was numerically rotated during each averaging period by applying a

double rotation, aligning the longitudinal wind component into the main wind direction

and forcing the mean vertical wind speed to zero (Kaimal & Finnigan 1994; Wohlfahrt *et*

al. 2008). Frequency response corrections were applied to raw eddy fluxes accounting for

low-pass (lateral and longitudinal sensor separation, sensor time response, scalar and

vector path averaging) and high-pass (block averaging) filtering (Massman 2000,

Massmann 2001) using a site-specific cospectral reference model (Massman & Clement

2004; Wohlfahrt *et al.* 2005). Experimentally-derived frequency response correction

factors (Aubinet *et al.* 2000, 2001) were used to assess the validity of the theoretical low-

pass filtering correction method, as detailed in Wohlfahrt *et al.* (2005). Finally, fluxes were corrected for the effect of air density fluctuations following Webb *et al.* (1980).

Half-hourly flux data were quality controlled in a five-step filtering procedure. First, periods were identified when the EC system was not working properly due to adverse environmental conditions (usually rain) or instrument malfunction. Second, half-hourly values that were comprised of less than the full compliment of measured values (i.e. less than 18,000) were removed. Third, data were subjected to the integral turbulence test (Foken & Wichura 1996) and accepted only on the condition that they did not exceed the target value (Foken *et al.* 2004) by more than 60% (Wohlfahrt *et al.* 2008). This occurred mostly for flow from the sector where the instrument tower was located. Fourth, data were subjected to the angle of attack test (β - beta; the angle between the wind vector and horizontal) which identifies errors in data resulting from the imperfect cosine response of sonic anemometers. Data were excluded when the angle of attack was greater than 20° (Geissbühler *et al.* 2000; Gash & Dolman 2003). Finally, data were excluded when the automatic gain control (AGC) of the IRGA was greater than the specific baseline value for each instrument. Increases from baseline AGC typically result from rain, snow, or ice accumulation on the surface of the lens of the IRGA and results in errors in water vapor density values.

The validity of the EC ET data was evaluated by calculating the degree to which EC measurements were able to close the ecosystem energy balance using the method described in Hammerle *et al.* (2007). Briefly, this method involves comparing the sum of turbulent heat fluxes—final latent (LE) and sensible heat (H) fluxes—calculated using EC data for each half-hour sampling period, to the available energy, or the difference

between net radiation (R_n) and soil heat flux (G), calculated for each half-hour sampling period. Annual energy balance closure for each site was calculated as the slope of the best-fit regression line of LE+H on R_n-G using all half-hourly values from the study year expressed as a percentage. Annual energy balance closure calculated for the study year across all sites was 94% (SV4: 108%; SV5: 97%; SV6: 93%; SV7: 79%; Fig. 2) these high closure values indicate a high degree of methodological certainty in EC ET estimates for all sites. Values greater than 100% may occur because of overestimation of soil heat fluxes, where we assumed a uniform soil bulk density of 1,400 kg m^{-3} (Devitt *et al.* 2008), soil particle density of ca. 2,600 kg m^{-3} (Gee & Or 2002), and soil organic matter content (0%) for all sites in Spring Valley.

Gap filling, ET calculations, and uncertainty analysis

Data gaps for each site, less than one day, resulting from filtering or missing data were filled using a site-specific regression equation of ET on daytime PFD (photon flux density [PFD] of photosynthetically active radiation [PAR]). For cases where data gaps were greater than one day (only occurring at SV5 and SV7), site-specific regression equations with PAR as the independent variable were used to gapfill both daytime and nighttime ET. Gaps greater than one day only occurred at sites SV5 (one 8-day period, one 9-day period) and SV7 (one 3-day period). Over the one-year study, only 1.5 to 3.1% of all half-hourly EC ET values were gap-filled for any of the sites. Total daily ET was calculated by summing each day's 48 (gap-filled) half-hourly records. Cumulative ET for the study period (20 April 2007 to 20 April 2008) was calculated by summing all original and gap-filled half-hourly values. Systematic uncertainty of ET estimates (e.g. Wohlfahrt
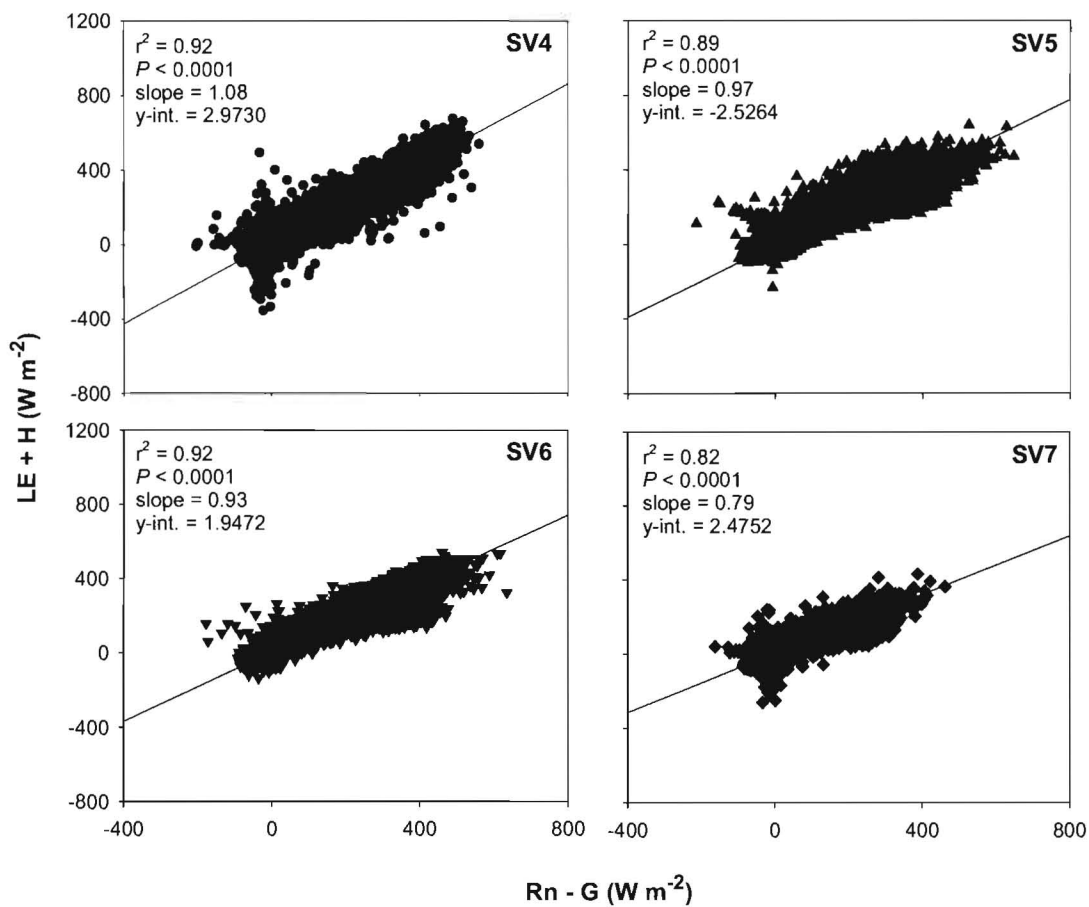
Figure 2. Energy balance closure for all EC ET sites located in Spring Valley, NV between 20 April 2007 and 20 April 2008.

et al. 2008) derive primarily from the collective effects of inherent instrument

measurement errors on the large density corrections (Webb *et al.* 1980, WPL) that need

to be applied to half-hourly EC ET values when measuring ET with open-path sensors

under conditions of large sensible heat exchange. In these situations, the effects of

concurrent air temperature and humidity fluctuations on H_2O densities (ρ_v) must be taken

into account. The uncertainty introduced by applying the WPL correction under the range

of inherent measurement errors for each instrument (sensor) was estimated by defining a

likely relative uncertainty for each independent parameter (instrument measurement) and

by applying this in turn to calculate annual ET (see Wohlfahrt *et al.* 2008). Assuming that

the various component uncertainties are independent, the combined uncertainty due to the

WPL correction was calculated by taking the square root of the sum of the squared

individual uncertainties.

Based on manufacturers' specifications, and on past experience with long-term

sensor stability, the water vapor density, and static air pressure were assigned

uncertainties of 10% (Wohlfahrt *et al.* 2008) while air temperature was assigned an

uncertainty of 2% (**Table 2**). Uncertainty in the sensible heat flux may arise from the fact

that the sensible heat flux was measured based on speed of sound measurements, which

has been shown by Loescher *et al.* (2005) to deviate from sensible heat flux derived from

measurements of air temperature with a fast-response platinum resistance thermometer by

up to 10% for this specific sonic anemometer model. On the other hand, Ham & Heilman

(2003), again for the same anemometer model used in this study, found extremely good

correspondence between sonic- and thermocouple-derived sensible heat flux

measurements. Additional uncertainty of the sensible heat flux arises from the choice

Table 2. Estimates of systematic uncertainty of annual ET (mm) calculated as the square root of the sum of the squared individual sources of uncertainty using density corrected data (Webb *et. al.*, 1980).

Source of uncertainty		SV4	SV5	SV6	SV7
T_{air}	(2%)	0.27	0.09	0.09	0.04
$\square_v$	(10%)	1.34	1.66	1.75	0.52
P	(10%)	0.29	0.13	0.14	0.07
F_H	(5%)	0.82	0.76	0.82	0.29
F_{H2O}	(5%)	28.50	8.21	8.16	5.10
Total systematic uncertainty		± 28.53	± 8.31	± 8.31	± 5.2

of coordinate system (Lee *et al.* 2004) and from the necessary (small) frequency response

corrections (Massman 2001). Based on the evidence presented above and some

preliminary sensitivity tests with different coordinate systems (data not shown), a 5%

uncertainty for the sensible heat flux was assumed. Similar to the sensible heat flux, a 5%

uncertainty for latent heat flux was assumed, intended to reflect uncertainties due to

choice of the coordinate system and frequency response corrections, which are based on a

site-specific cospectral reference model (cf. Massman & Clement 2004; Wohlfahrt *et al.*

2005) and have been validated against experimentally derived frequency response

correction factors following Aubinet *et al.* (2000) and Aubinet *et al.* (2001) as described

in Wohlfahrt *et al.* (2005) and Wohlfahrt *et al.* (2008). Based on this information our

choice of 5% uncertainty is justified and not nearly as large as the upper range of

potential errors in frequency response correction factors (30%) reported by Massman &

Clement (2004).

EC tower footprint analysis

       The footprint for each site, or area sampled by each EC tower during the study

year, was calculated using the footprint model of Hsieh *et al.* (2000) to estimate the

upwind distance and compass direction that represented 90% of the surface flux for each

half-hour period ($X_{90\%}$):

$$X_{90\%} = \frac{-D\,|\,L\,|^{(1-P)}\,Z_u^{P}}{k^2\,\ln(0.90)} \qquad\qquad \text{Eq. 1}$$

where k is the von Karman constant (0.4), L is the Obukhov length, and Z_u is the length

scale calculated as:

$$Z_u = \frac{Z_m\, u\, k}{u_*}$$ Eq. 2

where Z_m is the measurement height, u is the mean wind speed, and D and P are stability-dependent coefficients, i.e.

$D = 0.28$; $P = 0.59$ for unstable conditions

$D = 0.97$; $P = 1.00$ for near-neutral conditions

$D = 2.44$; $P = 1.33$ for stable conditions

Each calculated point, or footprint distance and direction, was then plotted in ArcGIS and a polygon was circumscribed on the outside of the collective set of points for the day before, during and after satellite acquisition, as well as a collective annual ET footprint. The polygon footprints were overlaid onto the Landsat TM satellite image for each site (**Fig. 3**) using the Region of Interest (ROI) tool, and an average vegetation index value was calculated (see '*Comparison of eddy covariance ET and remotely sensed vegetation indices*' for further information). The collection of plotted points for the study year was also used to construct a 3D-mesh plot of each footprint land area that shows the contribution of various parts of the footprint to ET fluxes (**Fig. 4**) and to calculate the number of points for each upwind distance from the EC tower that contributed to ET fluxes (**Table 3**).

ET measurements with dome static chamber

To compare EC ET estimates for validation and calibration, ET fluxes were measured within the immediate neighborhood (within 200 m) of each EC tower on 5 to
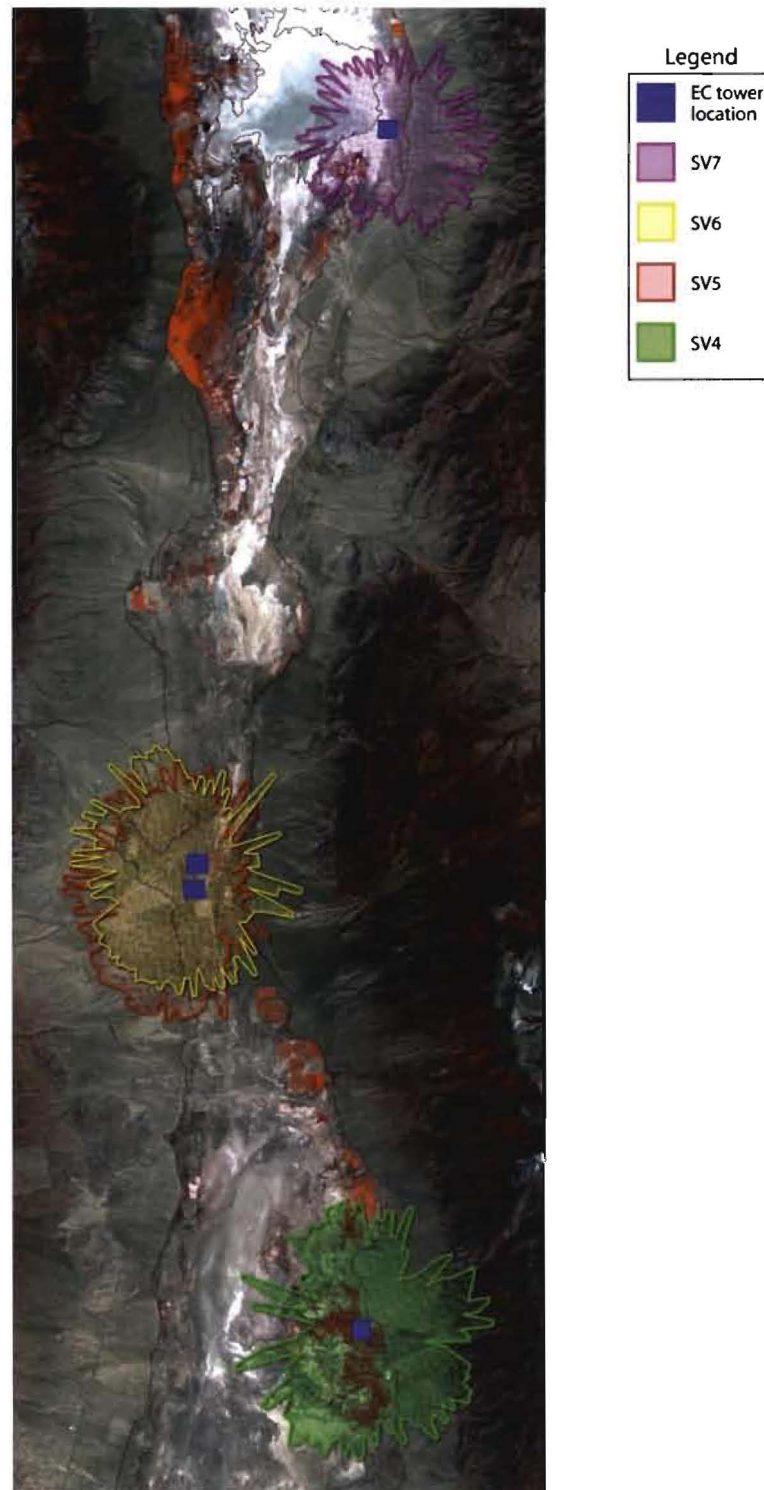
Figure 3. Landsat TM 5 image (June 16, 2007) of Spring Valley in eastern Nevada, USA showing the location of study sites (blue squares) with maximum annual footprint depicted around each EC tower.

a   **b**
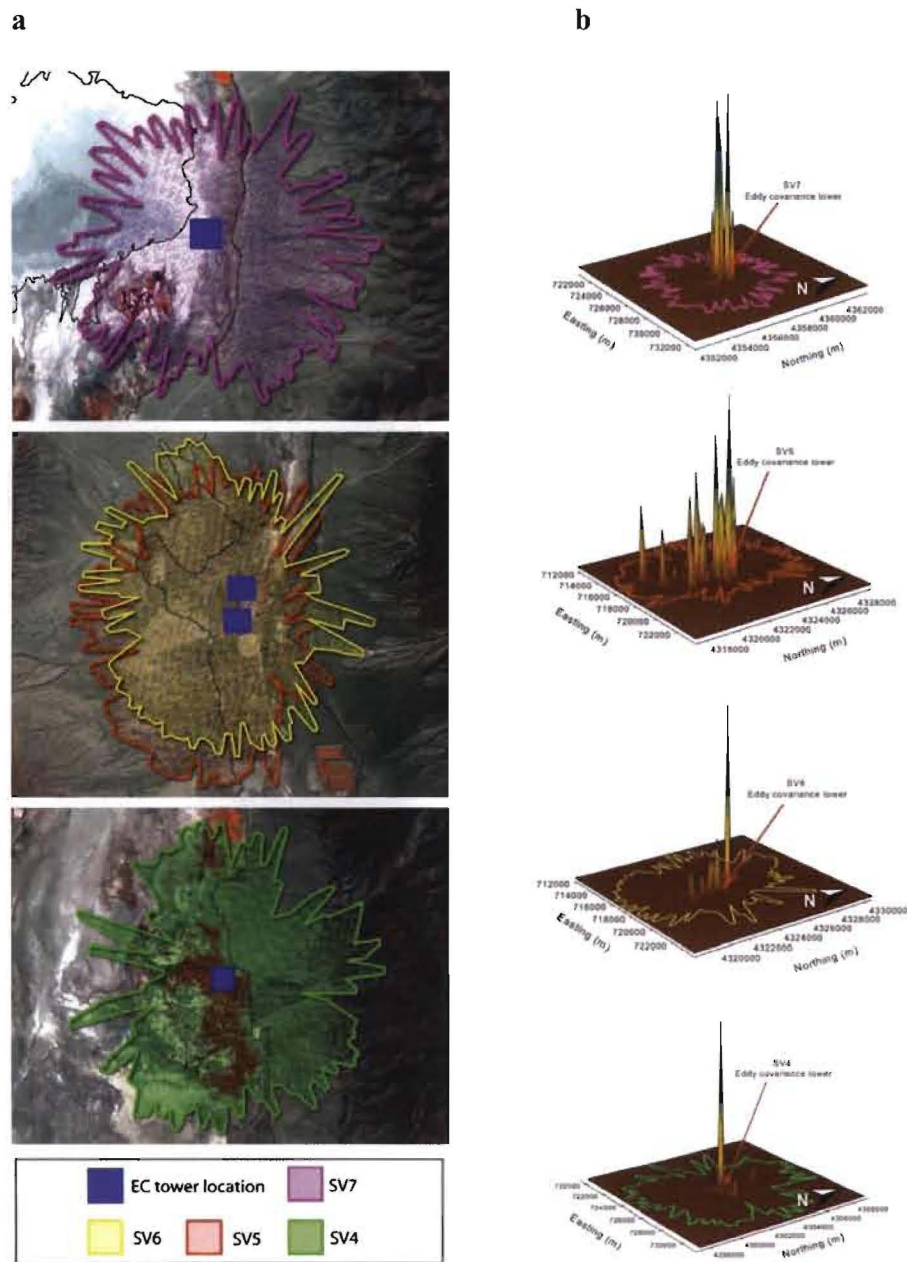
Figure 4. Landsat TM 5 image of each site showing maximum annual footprint depicted around each EC tower for sites SV7, SV6 & SV5, and SV4 (bottom panel) (**a**); and corresponding 3D-mesh images showing the level of representation of each 250 x 250 m pixel within each EC tower footprint to annual ET over the study year (**b**). Maximum annual footprint is the total area that contributed to 90% of the ET fluxes during the one-year study. The areas closest to each EC tower still contributed the most to annual ET (see: 3D mesh images in **b** and **Table 3**).

Table 3. Cumulative percentage of all EC ET values measured that derived from increasing radial distances from the EC tower for each site during the study year (20 April 2007 to 20 April 2008) in Spring Valley, Nevada, USA.

Distance from EC tower (radius m)	SV4 30 min. EC values within footprint (%)	SV5 30 min. EC values within footprint (%)	SV6 30 min. EC values within footprint (%)	SV7 30 min. EC values within footprint (%)
<100	12	3	4	10
<200	27	11	14	23
<300	38	21	25	33
<400	46	36	46	44
<500	51	61	64	57
<600	56	66	69	72
<700	61	70	73	78
<800	65	73	76	82
<900	68	76	78	85
<1000	72	78	81	87
<2000	90	91	92	96
<3000	95	95	96	98
<4000	97	97	97	99
<5000	98	98	98	
<6000	99	99	99	

15 representative 12.3 m^2 plots using a large static chamber (Arnone & Obrist 2003; Obrist *et al.* 2003; Jasoni *et al.* 2005). ET fluxes were measured over two (SV4, SV5, SV6) or three (SV7) 36-hour periods from May 30 to August 21, 2007 when shrub foliage was green (i.e. actively transpiring). Briefly, this method involves sealing the dome over each plot for 3 minutes, measuring the rate of change in the water vapor density inside the dome with an open-path infra-red gas analyzer (LI-COR LI-7500) operating at 10 Hz with 1-second averages logged using a laptop PC, and adjusting this rate by accounting for the volume of the dome, the area covered by the dome, and changes in air temperature and air pressure during the 3-minute measurement period. Only the initial linear portion of the change in water vapor concentration inside the dome during each 3-minute period is used to calculate ET; typically this was the first 20 to 40 seconds, but sometimes longer time periods at night when water vapor fluxes were low.

Comparison of ET measurements using EC and dome static chamber

Each ET rate (mm 30 min^{-1}) calculated for each dome sampling plot was first normalized by multiplying the ET rate by the percent vegetation cover (see method in Cablk & Kratt 2007) that fell within the EC tower footprint area specifically calculated for each 24 to 36 hour dome ET sampling period (**Figs. 5 – 8**), and then dividing by the percent vegetation cover measured within each dome plot. Normalized values, converted from measurement units of mmol H_2O m^{-2} s^{-1} to units of mm H_2O half-hour^{-1}, were then plotted with the mean half-hourly EC ET values. Individual half-hourly EC ET values for each site and sampling date were also plotted on corresponding dome ET values. In cases

Figure 5. EC tower footprint for site SV4 calculated for two dates corresponding to the area of each site simultaneously sampled using the static chamber dome. The orange line circumscribes the footprint corresponding to the June and July 2007 sampling dates. The red symbol represents the position of the EC tower. The green symbols represent the locations of the half-hourly EC ET mean values from the June sampling, and the orange symbols represent the locations of the half-hourly EC ET mean values from the July sampling. All symbols and lines are overlain on a 1 m resolution IKONOS image acquired between September and December 2005.

Figure 6. EC tower footprint for site SV5 calculated for two dates corresponding to the area of each site simultaneously sampled using the static chamber dome. The orange line circumscribes the footprint corresponding to the June and July 2007 sampling dates. The red symbol represents the position of the EC tower. The green symbols represent the locations of the half-hourly EC ET mean values from the June sampling, and the pink symbols represent the locations of the half-hourly EC ET mean values from the August sampling. All symbols and lines are overlain on a 1 m resolution IKONOS image acquired between September and December 2005.
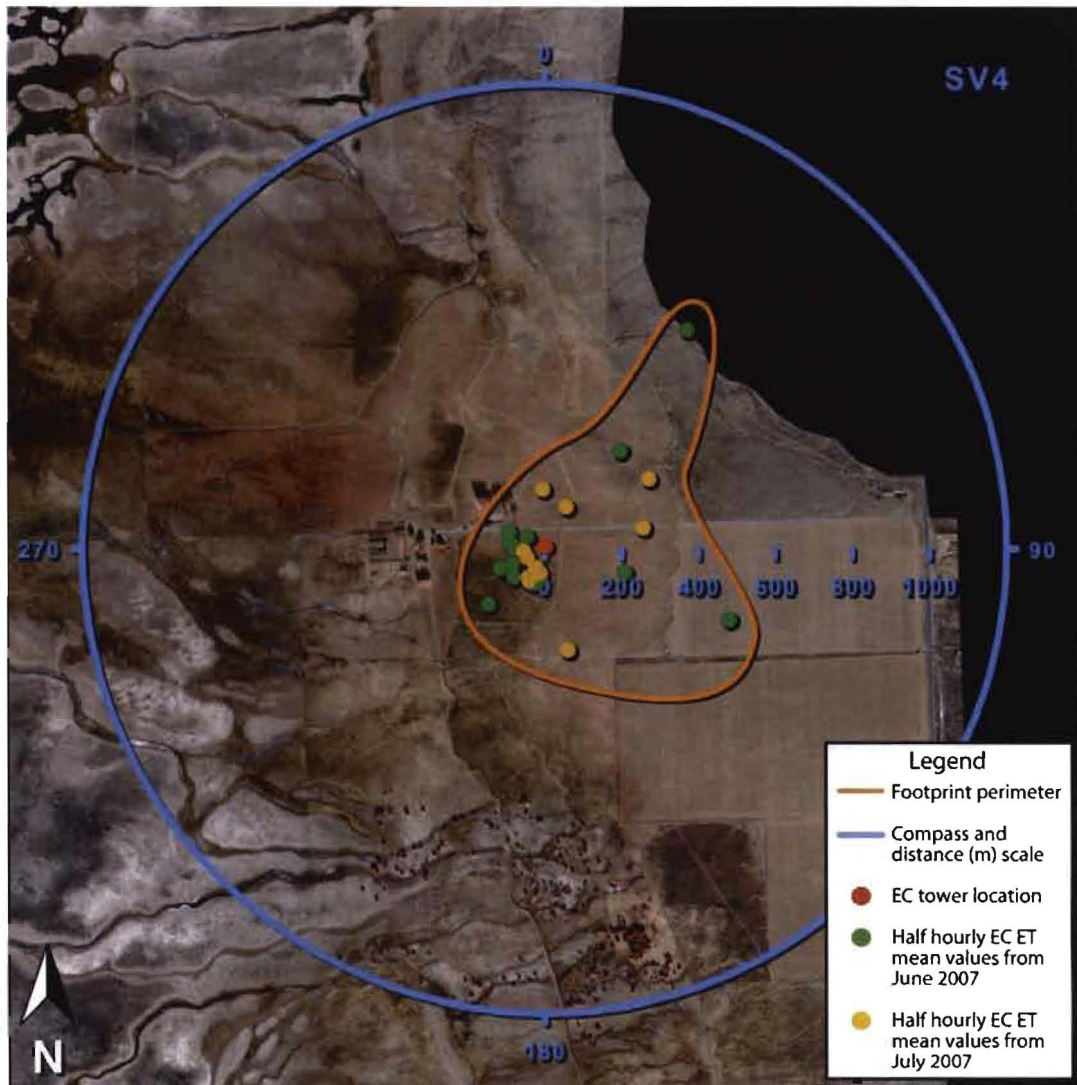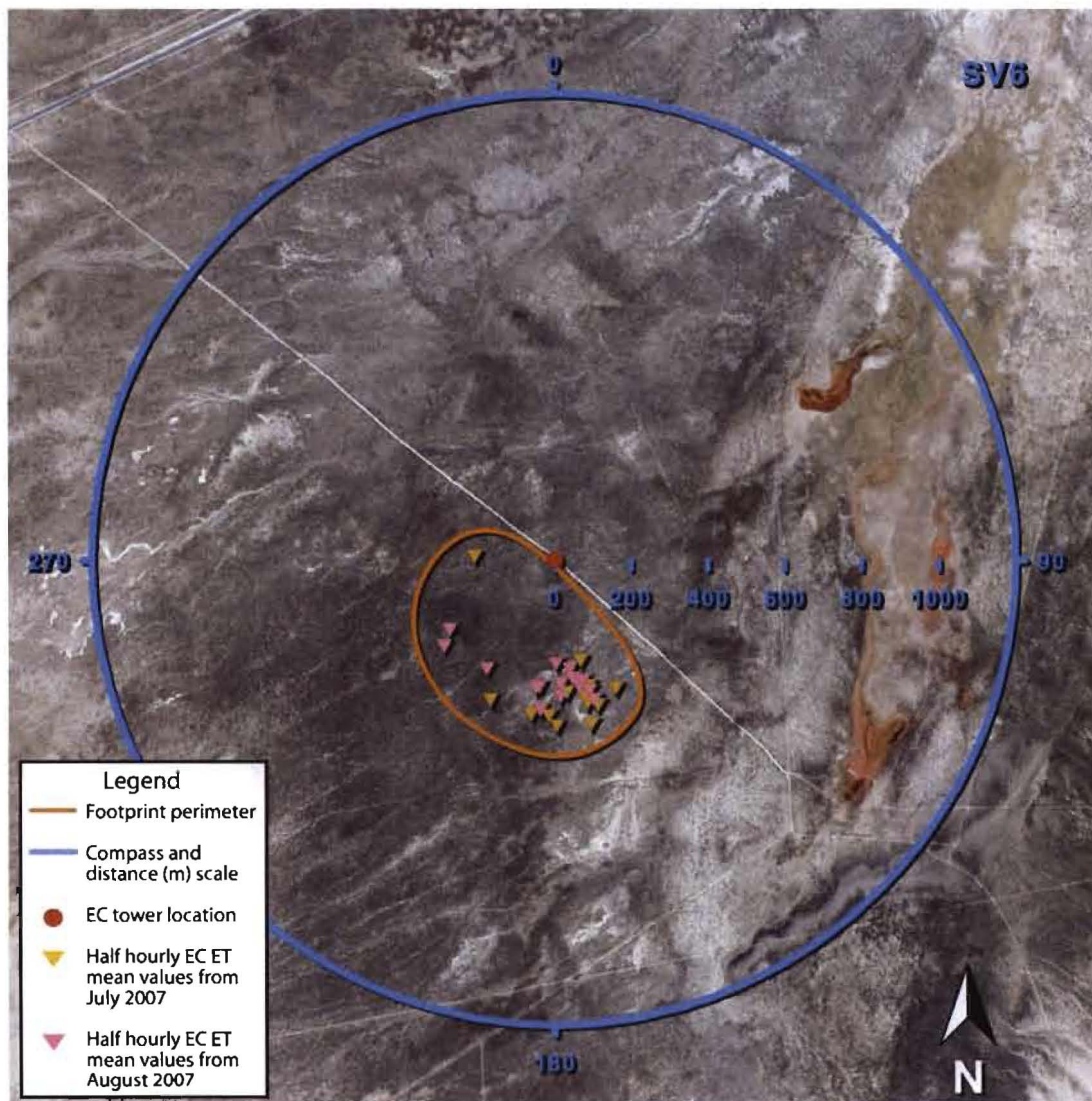
Figure 7. EC tower footprint for site SV6 calculated for two dates corresponding to the area of each site simultaneously sampled using the static chamber dome. The orange line circumscribes the footprint corresponding to the June and July 2007 sampling dates. The red symbol represents the position of the EC tower. The orange symbols represent the locations of the half-hourly EC ET mean values from the July sampling, and the pink symbols represent the locations of the half-hourly EC ET mean values from the August sampling. All symbols and lines are overlain on a 1 m resolution IKONOS image acquired between September and December 2005.
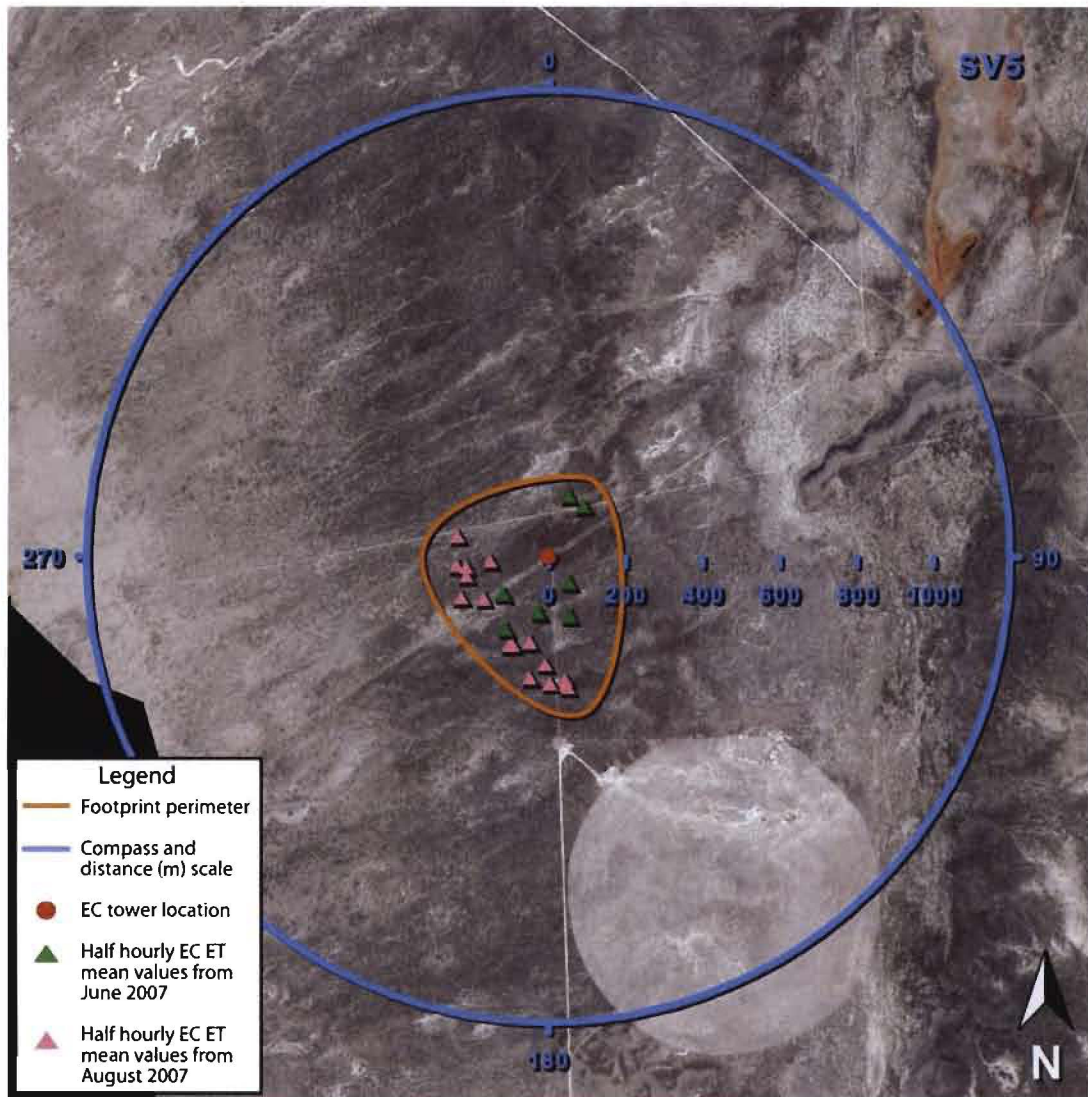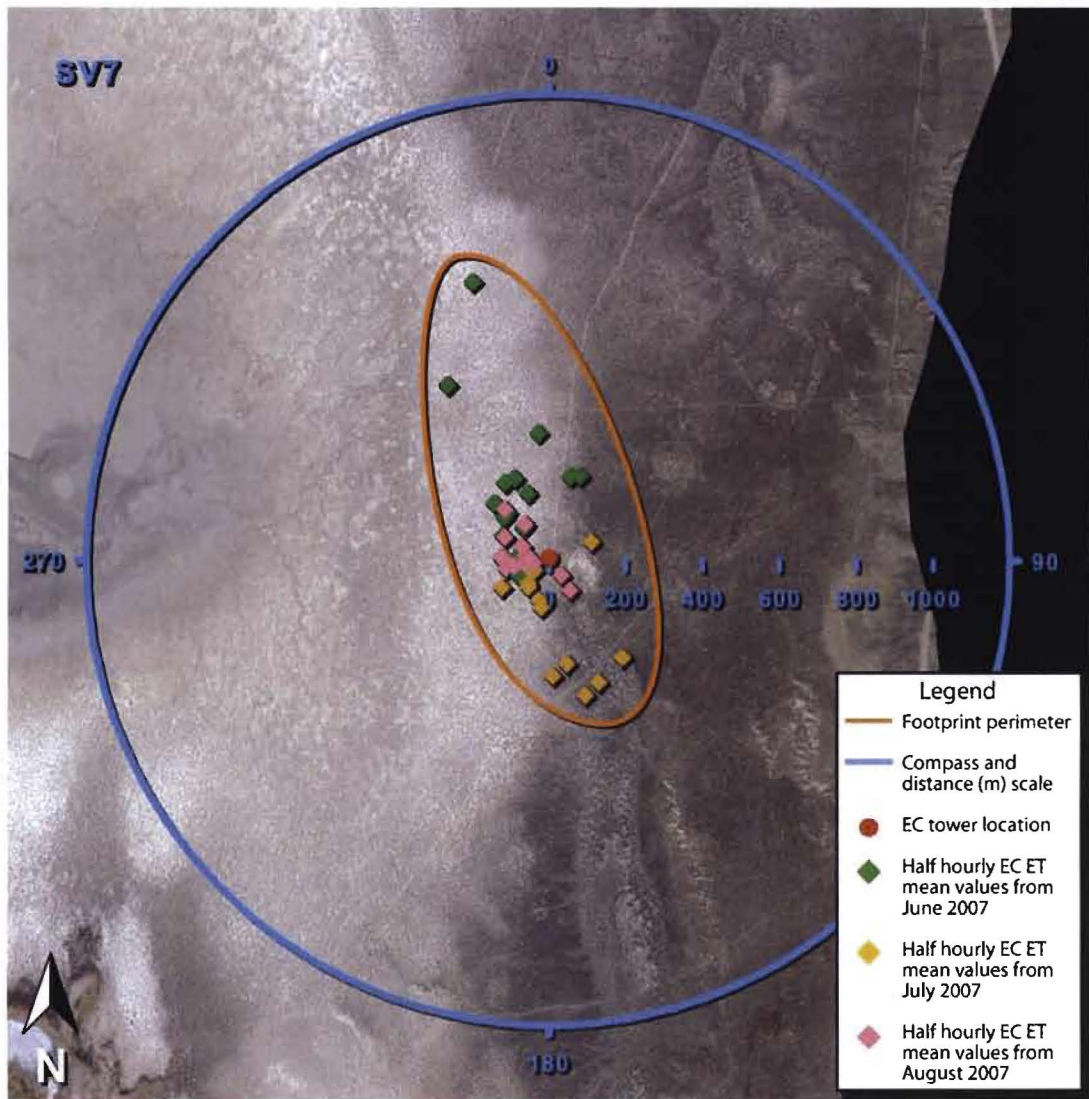
Figure 8. EC tower footprint for site SV7 calculated for three dates corresponding to the area of each site simultaneously sampled using the static chamber dome. The orange line circumscribes the footprint corresponding to the June and July 2007 sampling dates. The red symbol represents the position of the EC tower. The green symbols represent the locations of the half-hourly EC ET mean values from the June sampling, the orange symbols represent the locations of the half-hourly EC ET mean values from the July sampling, and the pink symbols represent the locations of the half-hourly EC ET mean values from the August sampling. All symbols and lines are overlain on a 1 m resolution IKONOS image acquired between September and December 2005.

where more than one dome ET value occurred within a half-hourly EC measurement

period, the mean of multiple dome ET values was used. EC ET data (within the footprint

during the time of dome sampling) were then linearly regressed on corresponding values

of dome ET.

Comparison of static chamber dome ET and plant canopy greenness

To evaluate the potential for using a visible-light plant canopy greenness index

(percentage of land area covered by green vegetation) to predict ET, dome ET values

were compared with bird's eye view color photographs of each dome plot taken at each

sampling date with a 8-megapixel Canon A630 color digital camera. Greenness index

was calculated by printing each digital photograph on 22 x 28 cm paper, overlaying a 2.4

x 2.4 cm transparent grid, counting the number of grid cells that were at least 50% green,

and expressing this as a percentage of the total number of grid cells. Dome ET values

were then linearly regressed (Jasoni *et al.* 2005) on corresponding plant canopy

percentage greenness values for each site and date, as well as for all sites and all dates.

Comparison of eddy covariance ET and remotely sensed vegetation indices

Georectified, terrain corrected (EROS 2006) 25-m resolution, Landsat 5 Thematic

Mapper (TM) images were acquired for the same satellite path/row (39/33) for every

cloud-free pass (passes are 16 days apart) during the 2007 growing season. Specifically

for this study, images were acquired on eight dates, which included April 29, May 15,

May 31, June 16, July 2, July 18, August 19, and September 20. Landsat TM images are

comprised of six visible and near infrared bands plus a thermal band. Path/Row 39/33

images, which encompassed nearly all of Spring Valley, were used to develop regression relationships between ET and vegetation indices (Normalized Difference Vegetation Index [NDVI], Enhanced Vegetation Index [EVI]) for each image acquisition date and site. Regression relationships between mean growing season vegetation indices and total annual ET (April 2007 to April 2008) were also developed by combining data from all four sites. Images were first calibrated to top-of-atmosphere radiance using the ENVI (Environment for Visualizing Images, ITT Visual Information Solutions, Boulder, Colorado, USA) Landsat TM 5 calibration subroutine (Chander & Markham 2003). The empirical line method and field-based spectra representing a range of light to dark non-vegetated surfaces (Farrand *et al.* 1994; Smith & Milton 1999) were used to atmospherically correct images while simultaneously normalizing and converting pixel data numbers to ground reflectance values. ENVI and SigmaStat (Systat Software Inc., San Jose, California, USA) software packages were used to analyze images.

Two vegetation indices (NDVI and EVI) were shown previously to be reasonable predictors of green vegetation cover and correlated with ET in other arid regions (e.g. Tucker 1979, Nagler *et al.* 2007, Groeneveld *et al.* 2007). NDVI has been widely used and is the most frequently published vegetation index. EVI, which includes a blue band and two coefficients, in addition to the red and near infrared bands, was recently shown to be highly correlated with ET in arid regions (Nagler *et al.* 2005 and Nagler *et al.* 2007). Because EVI includes a blue band, it minimizes atmospheric and soil background influences and is considered to be more sensitive to high canopy covers than NDVI, which is known to saturate with dense canopy cover (Huete *et al.* 2002). NDVI and EVI were calculated as follows:

$$NDVI = (R_{NIR} - R_{RED}) / (R_{NIR} + R_{RED}) \qquad\qquad Eq.\ 3$$

(Rouse *et al.* 1974)

$$EVI = 2.6 * (R_{NIR} - R_{RED}) / (R_{NIR} + (6 * R_{RED}) + (7.5 * R_{BLUE}) + 1.0) \qquad Eq.\ 4$$

(Nagler *et al.* 2007)

where R is the reflectance for the waveband indicated by each subscript, NIR is the near infra-red waveband from 0.76 to 0.90 nm, RED is the waveband from 0.63 to 0.69 nm, and BLUE is the waveband from 0.45 to 0.52 nm.

Extrapolating eddy covariance ET to whole-valley lowland ET using remotely sensed vegetation indices

To evaluate the potential for using the NDVI or EVI predicted ET for Spring Valley, and to upscale the EC ET measurements to whole-valley scales, EC ET measurements at each of the four sites were linearly regressed on NDVI/EVI of the actual footprint area sampled by the EC tower on (a) the entire day before the Landsat TM satellite passed over each site; (b) the day that the satellite passed over the site; and (c) the day after the satellite passed over the site. The mean total daily ET flux calculated for all three days was also compared with the mean NDVI/EVI footprint value calculated for these days to buffer the sometimes strong day-to-day variation in daily ET. These calculations assume that NDVI/EVI of a particular footprint area changes little over a two- to three-day period. The TM satellite provided usable (e.g. cloud- and snow-free) spectral data on eight dates in 2007 that spanned the growing season (April 29, May 15 and 31, June 16, July 2 and 18, August 19, and September 20) (see Appendix **Table A1** for mean growing season NDVI and EVI values). Regression fits were then explored for

individual sites and individual sampling days, individual sites across all sampling days, all sites for individual sampling days, and all sites across all sampling days.

Total annual ET (dome unadjusted annual EC ET) was also regressed on mean growing season NDVI and EVI across all sites to explore the relationships between ET and vegetation indices at longer, more highly aggregated temporal scale. To guard against the possible influence that anticipated high NDVI and EVI values of the grassland (SV4) site could have on the regression relationship used to extrapolate to ET for the whole basin which is dominated by shrublands with low NDVI/EVI values, annual ET for just the lower NDVI/EVI shrub sites (NDVI$\leq$0.13, EVI$\leq$0.055—see **Fig. 9**) was also regressed on the corresponding mean growing season NDVI, and EVI, values for these sites. Annual EC ET for the entire basin was calculated for each combination of regression equations by summing the annual ET calculated for each pixel and converting ET units of mm year^{-1} to acre feet year^{-1}.

Well construction and ground water fluctuations

Ground water levels and precipitation were monitored at each of the four sites as another means to estimate annual ET. In May 2007, monitoring wells were installed at each site. All wells were constructed using 0.18-m diameter hollow stem augers. Each auger flight was a nominal 1.5 m in length. Core samples, 0.60 m in length, were removed with a split-spoon sampler through the center of the hollow stem auger. Split spoon soil sampling minimizes the transfer of drill cuttings to the surface that may confound the accurate characterization of soil properties. Soil samples were removed
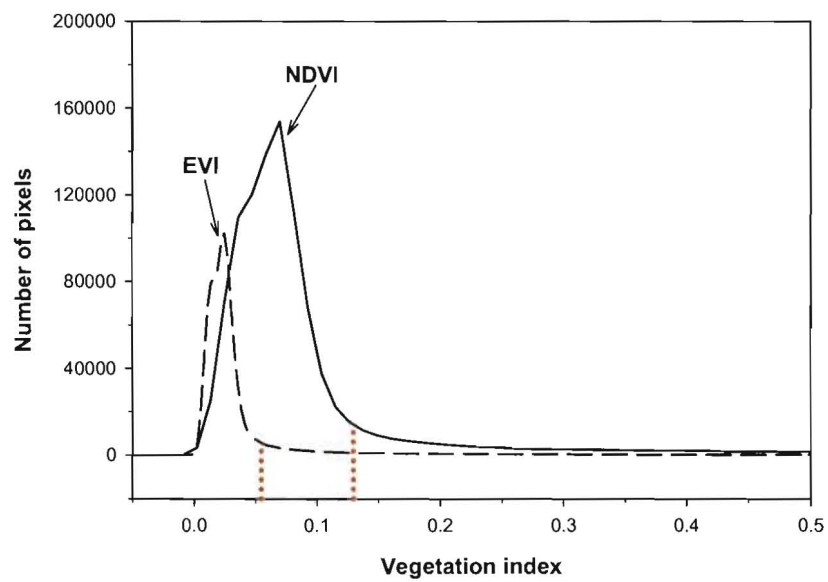
Figure 9. Frequency distribution of NDVI and EVI values by pixel count per NDVI/EVI range for all Landsat TM 5 (acquired in 2007) pixels in the phreatophytic zone of Spring Valley. The thresholds used for high NDVI/EVI values are demarcated with the drop-down red lines. Note that the class width for NDVI (0.0113 units) and EVI (0.0027 units) histograms are different.

immediately after coring (i.e. before drilling the next flight) and sealed in polyethylene

bags for textural analysis. The top 0.6 m of every 1.5 m layer of substrate (e.g. 0-0.6 m,

1.5-2.1 m, 3.0-3.6 m, etc.) to total drilling depth was sampled. After the saturated zone

was encountered, drilling was temporarily suspended until water level in the hole no

longer fluctuated. The time required for the water level to stabilize was used as an

estimate of hydraulic conductivity. Drilling and sampling was then resumed until the

auger tip was 4.1 m below the estimated static water level. Soil from the last 0.8 m of

each core was also sampled. A 5-cm diameter piece of schedule 40 PVC flush-joint pipe,

with a 15-cm long well point at the base, was inserted into the cored hole followed by 4.6

m of 20-slot screen and then sufficient blank well casing to reach ground surface. The

well screen was positioned so that 0.8 m of screen was above the static water level. The

PVC pipe and screen were lowered through the center of the hollow stem augers. As the

augers were removed, gravel pack material was poured into the annular space, filling it to

approximately 0.6 m above the upper screen slot. Bentonite aggregate (9.5-mm particle

diameter) was then packed over the gravel and then hydrated with water to create a 0.3-m

gap at the top of the annulus. The remaining annulus was filled to the surface with neat

cement. Details of well construction for each site (**Appendix Figs. A1** through **A4**), and

lithologic descriptions, are given in the Appendix. A surface level well protector was

placed over the top of the well and a concrete pad was poured to finish well construction.

Each well was equipped with a pressure transducer (Pressure Systems, Inc.,

Hampton, Virginia, USA) connected to the same data logger as used for the EC

equipment. All transducers were vented with a pressure range of 0 to 34 kPa gauge.

Pressure transducers were lowered into wells at SV5, SV6, and SV7, with about 2.7 m of

ground water head over the sensor. In well SV4, the transducer was lowered to about 2.4

m into the water column because the water level had not yet completely recovered

following drilling. Pressure was recorded every 60 minutes.

Daily, weekly and monthly changes in ground water level were calculated for

each site, and these values were compared with daily and cumulative daily EC ET values

to determine the feasibility of quantifying ground water extraction by phreatophytic (e.g.

greasewood, sagebrush, rabbitbrush) and putatively non-phreatophytic (grasses) plants

growing at the sites. All values are reported relative to depth below ground surface.

Results

Ecosystem ET

ET was measured at all sites using EC derived from a relatively large footprint

area around each tower and, thus, covered a sizable and representative piece of the local

ecosystem. For all sites, the fetch distance that encompassed at least 90% of all ET fluxes

during the year-long study extended out to 2,000 m from the tower, primarily in upwind

compass directions. Locations within 1,000 m from each EC tower contributed between

72% and 87% of all ET fluxes (**Table 3**). An average of ET flux values of 7%, 19%,

29%, 43% and 58% were measured within distances of 100, 200, 300, 400 and 500 m

from the towers, respectively.

ET measured at each site varied from day-to-day within a range of 0.7 mm d^{-1} at

SV4 and 0.3 mm d^{-1} at sites SV5-SV7 and showed large increases on days with and

immediately following precipitation (**Fig. 10**). Only site SV4—the agricultural grassland

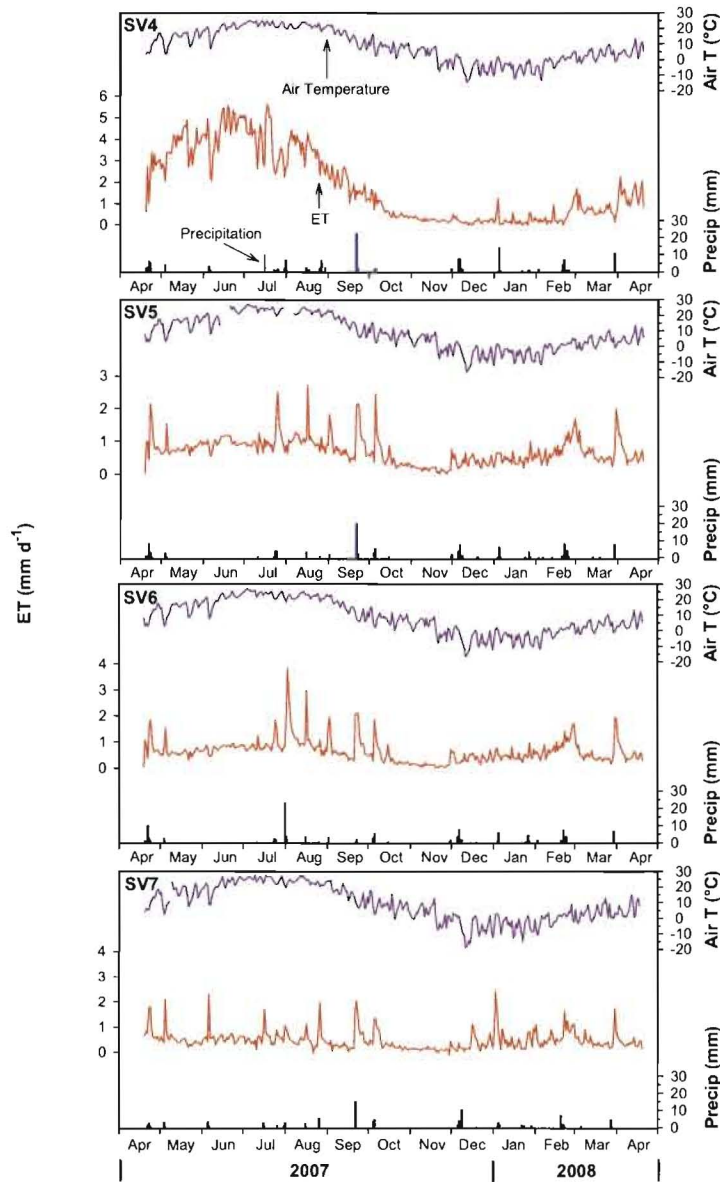site—exhibited seasonal changes in daily ET, with rates increasing from 1.5 to 1.9

Figure 10. Mean daily ET, mean daily air temperature, and mean daily precipitation for each eddy covariance site located within Spring Valley between 20 April 2007 and 20 April 2008. The solid red line (—) represents mean daily ET, the solid purple line (—) represent mean daily air temperature, and blue bars (▌) represent precipitation (mm d⁻¹).

mm d^{-1} in April 2007 to peak levels of 3.8 to 4.1 mm d^{-1} in June 2007. Daily ET

gradually decreased to about 0.1 mm d^{-1} by late October 2007 and remained at that level

through the winter. All three shrubland sites showed only slight seasonal fluctuations in

daily ET. The clear seasonal patterns observed at SV4 in daily ET reflected seasonal

patterns in grassland plant canopy development and senescence that corresponded to

changes in air temperature and PFD. Seasonal patterns in daily ET at the shrub sites

generally corresponded to seasonal patterns in air temperature (**Fig. 10**) and vapor

pressure deficit of air near plant canopies (data not shown), both of which also

corresponded to the apparent amount of green shrub foliage present (**Fig. 11**). Overall,

mean spring and summertime ET at SV4 exceeded ET measured at the shrub sites by

three- to four-fold. Differences in daily ET among sites translated into parallel

differences in cumulative ET (**Fig. 12**) and total annual ET (**Table 4**). Total ET for the

study period measured with EC was 659±29 mm, 260±8 mm, 238±8 mm, and 172±5 mm

for sites SV4, SV5, SV6 and SV7, respectively. Large diel oscillations in ET observed at

all sites during the growing season reflected diel patterns in air temperature but

corresponded more closely to PFD (Appendix Figures B, C, D and E). Oscillations in ET

observed at SV4 during the growing season were the largest among the four sites; for

example, oscillations were observed at SV4 from -0.05 to 0.0 mm half-hour^{-1} at night to

daytime peaks of between 0.2 to 0.4 mm half-hour^{-1}. Diel oscillations measured in colder

months at all sites were much smaller than those measured during the growing season.

Small negative latent heat fluxes were consistently observed at night at all sites,

indicating net water vapor uptake by the ecosystem through condensation under colder

nighttime air, plant and soil surface temperatures.
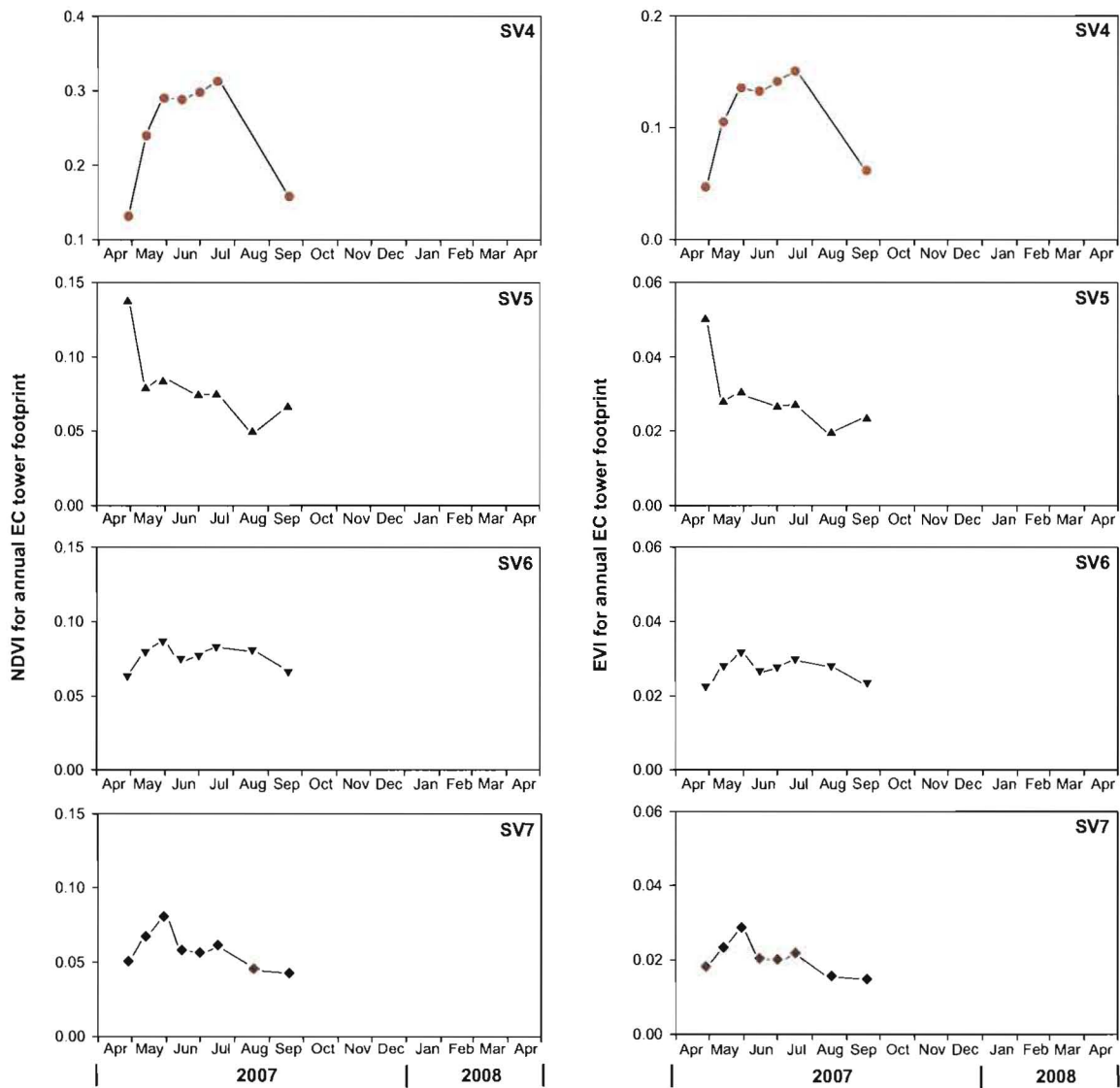
Figure 11. Seasonal patterns in NDVI (left column of graphs) and EVI (right column of graphs) of the annual EC tower footprints for the four study sites during the growing season of 2007 in Spring Valley, Nevada, USA. Note different scales used on y-axes.
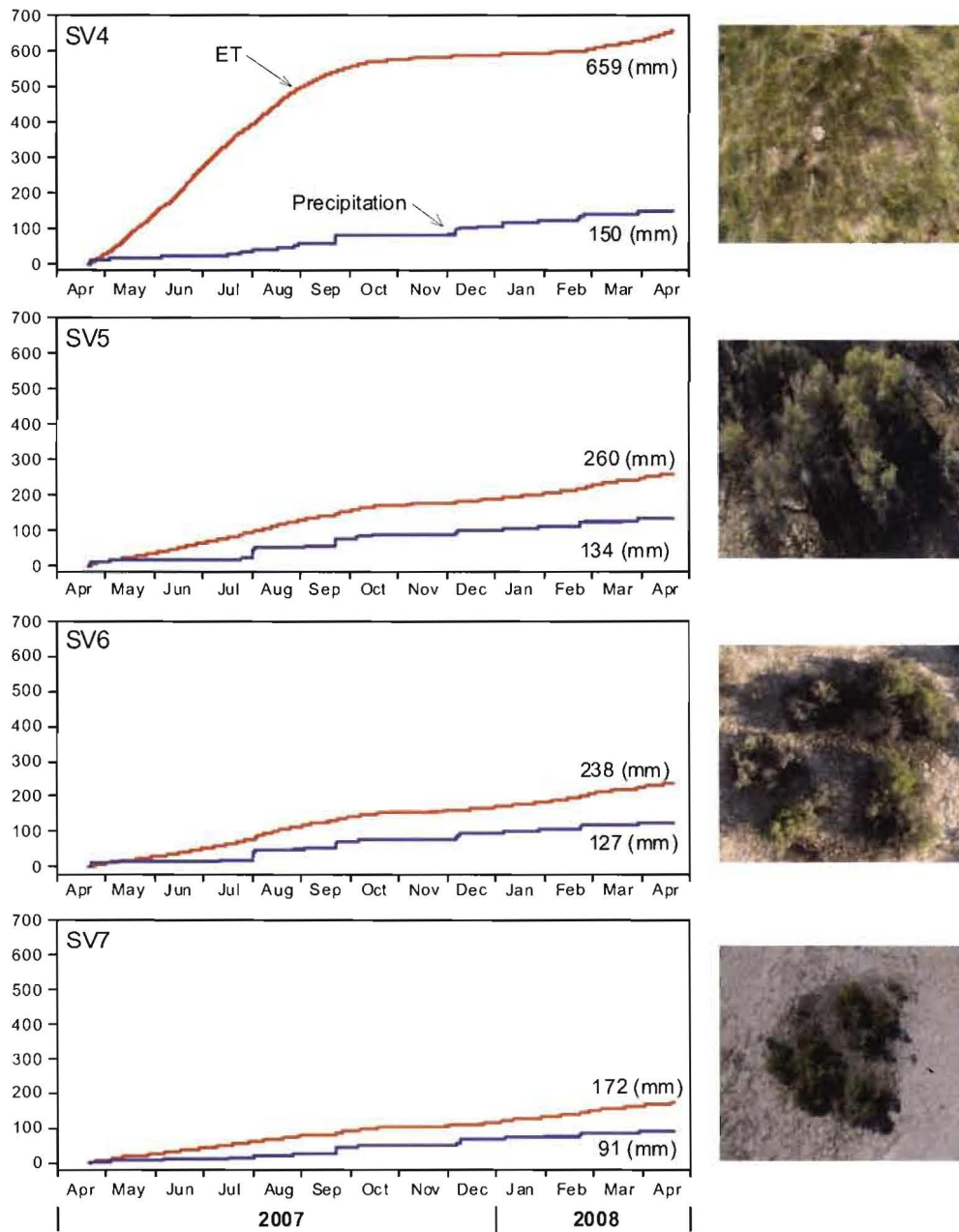
Figure 12. Cumulative ET and cumulative precipitation (30-minute time steps) for all four EC sites located within Spring Valley between 20 April 2007 and 20 April 2008. The solid red line (—) represents cumulative ET and the solid blue line (—) represents cumulative precipitation. Photographs to the right of each graph show the vegetation at that site.

Table 4. Annual ET measured at four lowland vegetated Great Basin sites in eastern Nevada, USA, using eddy covariance, EC, and adjusted annual ET for the same sites using (*i*) site-specific--**Figure 14a**, and (*ii*) all-site composite-**Figure 14b**--linear regression relationships (equations) between ET measured with EC and ET measured simultaneously with a large static chamber dome (using equations given in the individual panels of **Figure 14**).

Site	Annual EC-ET (mm)	Adjusted annual EC-ET (mm) (site-specific dome-ET on EC-ET)		Adjusted annual EC-ET (mm) (all site EC-ET on dome-ET)	
SV4	659 ± 28	437 ± 19	* -33.7	551 ± 23	* -16.4
SV5	260 ± 8	160 ± 5	* -38.6	217 ± 7	* -16.4
SV6	238 ± 8	155 ± 5	* -35.1	199 ± 7	* -16.4
SV7	172 ± 5	158 ± 5	* -8.3	144 ± 4	* -16.4

* Percentage differences from actual measured EC ET

Simultaneous comparison of ET measured with EC and static chamber dome

The correspondence between simultaneous EC ET and dome ET differed by site and sampling date (**Fig. 13** and **Fig. 14**). In general, estimates of dome ET were lower than ET measured using EC. Most of the differences between the two methods occurred during the day when ET was greatest (**Fig. 13**). Slopes of linear regressions of EC ET on dome ET ranged from 1.14 at SV7 to 1.70 at SV5 with SV4, SV5 and SV6 exhibiting similar slopes (**Fig. 14a**). Coefficients of determination (r^2 values) for regressions of within-site relationships between the two methods were relatively high, ranging from 0.70 to 0.87, as was correlation for the regression that included data from all sites and dates pooled together ($r^2 = 0.81$). Thus when viewed on a site-by-site basis (first adjusted EC ET column in **Table 4**) across all sampling dates, annual EC ET values adjusted using the site-specific relationship between dome ET and EC ET were 34%, 39%, 35% and 8% lower than unadjusted annual EC ET values, for sites SV4, SV5, SV6 and SV7, respectively. When viewed across <u>all</u> sites and sampling dates, agreement between the two methods improved significantly (**Fig. 14b**) with only a 16% downward adjustment in annual EC ET calculated for all sites (second adjusted EC ET column in **Table 4**).

Relationship between chamber-measured ET and plant greenness index

The relationship between dome ET and the corresponding plant canopy green cover (greenness index) of each 12.3 m^2 sampling plot was poor when viewed by individual site (**Fig. 15a**). The slope of regression lines for SV4, SV5 and SV6 were not statistically significant ($P>0.36$). At site SV7 where the relationship was significant ($P_{slope}=0.0417$), canopy greenness explained only 14% of the variability observed in ET.
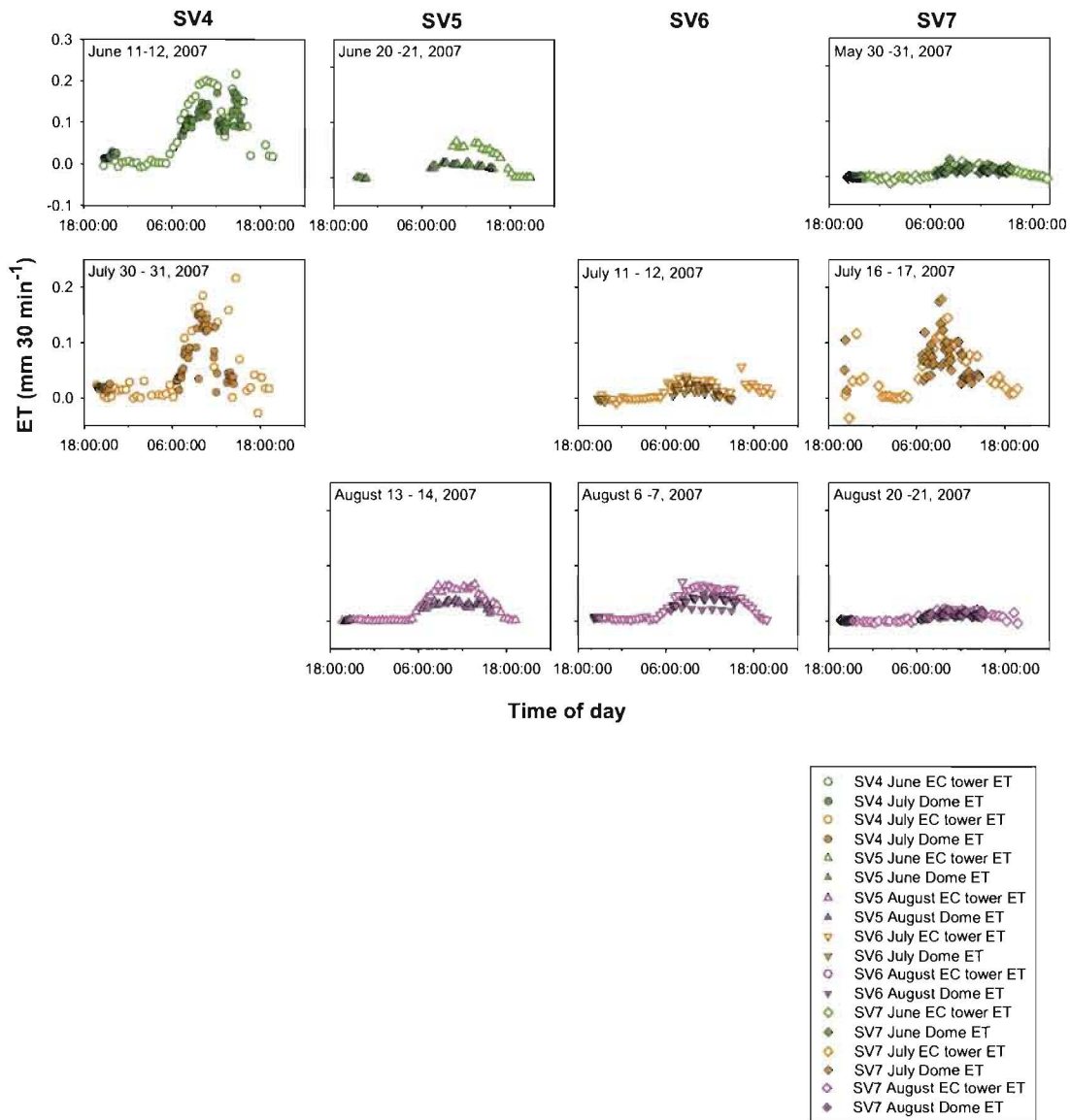
Figure 13. Diel time courses of ET measured with the EC tower (open symbols) and with the dome (filled symbols). Each ET value measured with the dome was adjusted to correspond to mean vegetation cover within each EC tower footprint during the time of dome sampling and to the mean vegetation cover within the specific dome plot being measured. Green symbols correspond to rates measured in June 2007, orange symbols to rates measured in July 2007, and pink symbols to rates measured in August 2007. Circles represent SV4; upward pointing triangles, SV5; downward pointing triangles, SV6; and diamonds, SV7. Gap in data between 20-21 June 2007 at SV5 was due to a malfunctioning CR5000 data logger.
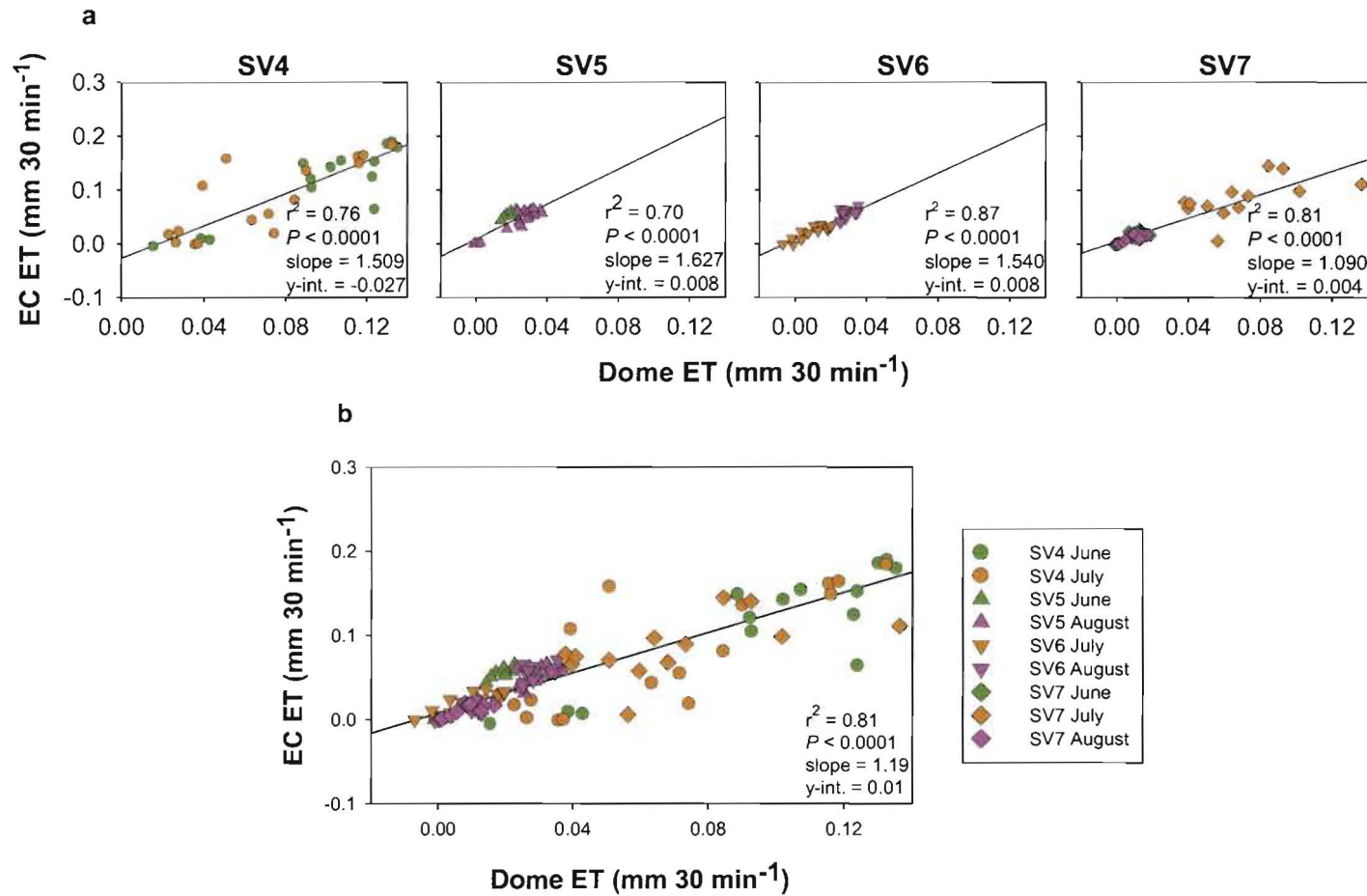
Figure 14. Simple linear regressions of EC ET rates on dome ET rates using 30-minute mean values for each site (**a**) and all sites pooled together (**b**).

a
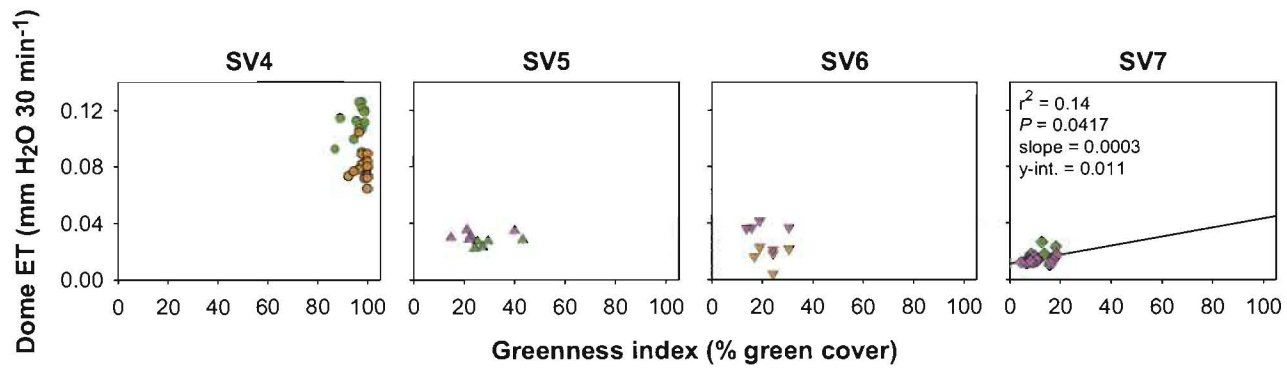
b
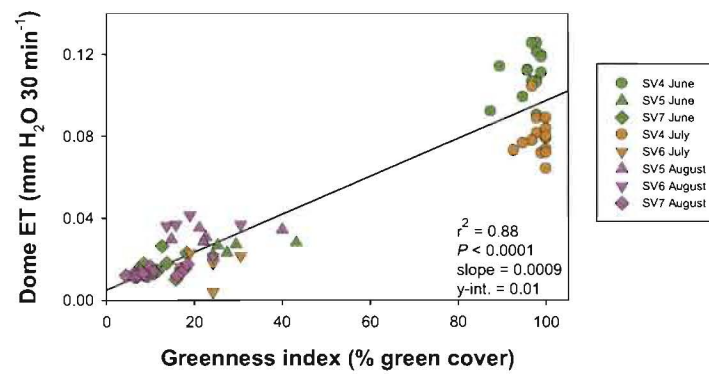
Figure 15. Relationship between mean daytime ET measured with the dome static chamber and percentage vascular plant green area cover for each site (**a**) and for all sites together (**b**) based on simple linear regressions.

Relationship between EC ET and vegetation indices (NDVI, EVI)

Overall seasonal patterns in daily ET (see **Fig. 10**) appeared generally to

correspond positively with early seasonal patterns in vegetation indices (NDVI and EVI,

Fig. 11). The relationship between total daily EC ET (over 24 hours) at each site and the

mean vegetation index (NDVI—**Fig. 16**, or EVI—**Fig. 17**) within the tower footprint that

corresponded to the day of, day before, and day after each pass of the Landsat TM

satellite for all available data-acquisition dates was not statistically detectable in most

cases (P_{slope}>0.10). NDVI and EVI also explained very little of the variation in daily and

three-day mean ET values (r^2 values between 0.00 and 0.25; graphs in **Fig. 16** and **Fig. 17**

with no regression lines depicted indicating P_{slope}>0.10). Only at site SV4 were linear

regressions statistically significant (P_{slope} range was 0.011 to 0.036, r^2 range was 0.62 to

0.76) for NDVI (or EVI) on ET measured on the day before image acquisition, and NDVI

(or EVI) on three-day mean ET. Similarly, relationships were significant between daily

vegetation indices (eight Landsat acquisition dates) and corresponding ET values when

all sites were included (site SV4 providing high ET and NDVI and EVI values).

However, because high NDVI/EVI agricultural grasslands only represent a small fraction

of the lowland parts of Spring Valley, and because of the poor relationship observed

between daily vegetation indices and ET for the dominant vegetation type in Spring

Valley we chose to rely on relationships between ET and vegetation indices over larger

temporal (annual) and spatial (annual EC tower footprint) scales with data from all sites

pooled. This pooling improved the relationships between vegetation indices and ET (**Fig.**

18) with mean warm season NDVI values spanning the range from 0.055 (SV7) to 0.136

(SV4). Regressions of total annual ET on mean warm season NDVI across all four sites
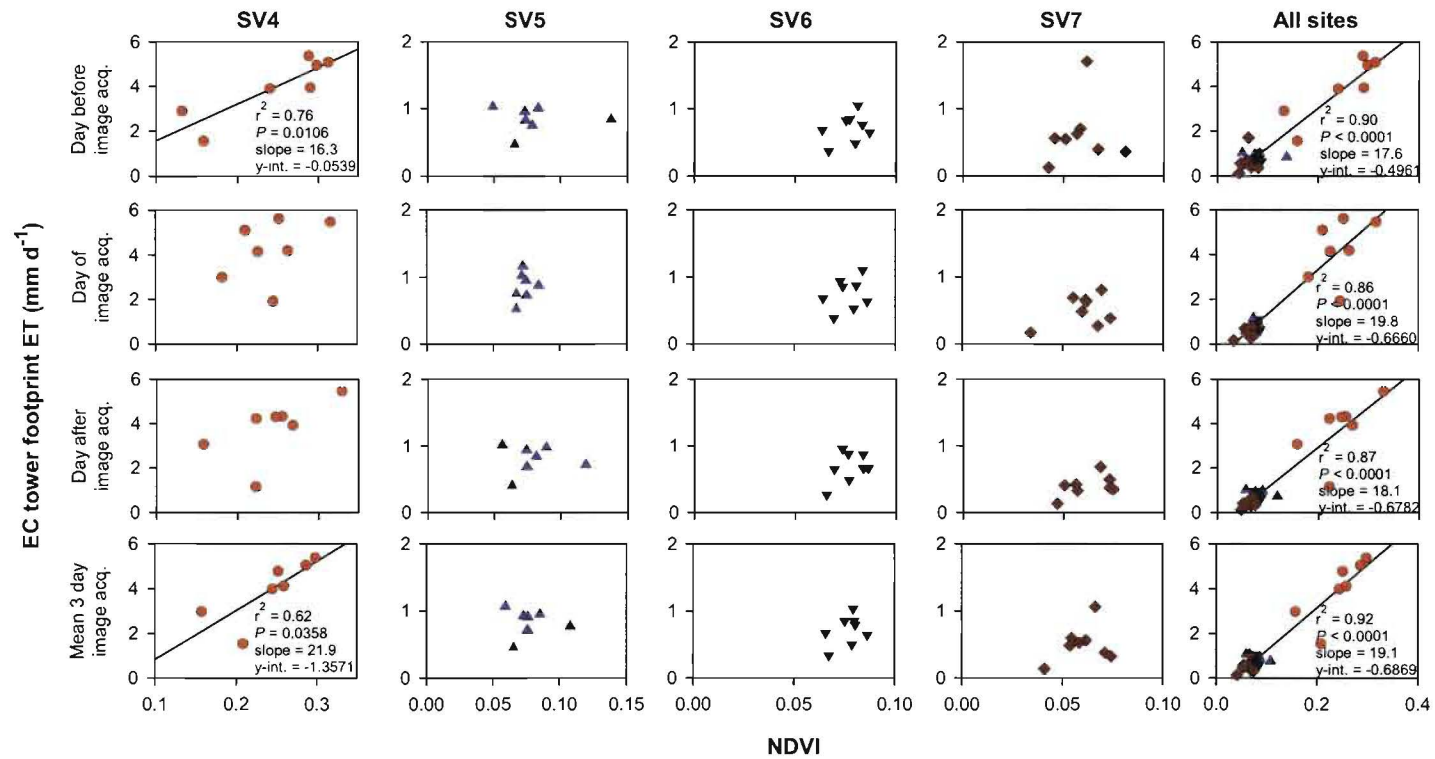
Figure 16. Relationships of daily ET (24-hour total) measured with EC on corresponding daily NDVI values calculated for the EC tower footprint of the day before, day of, and day after Landsat TM 5 image acquisition dates for each study site (SV4, SV5, SV6 and SV7). Each point in each panel represents the daily ET and NDVI value for each valid satellite sampling date. The row of panels on the far right represents all sites and sampling dates.
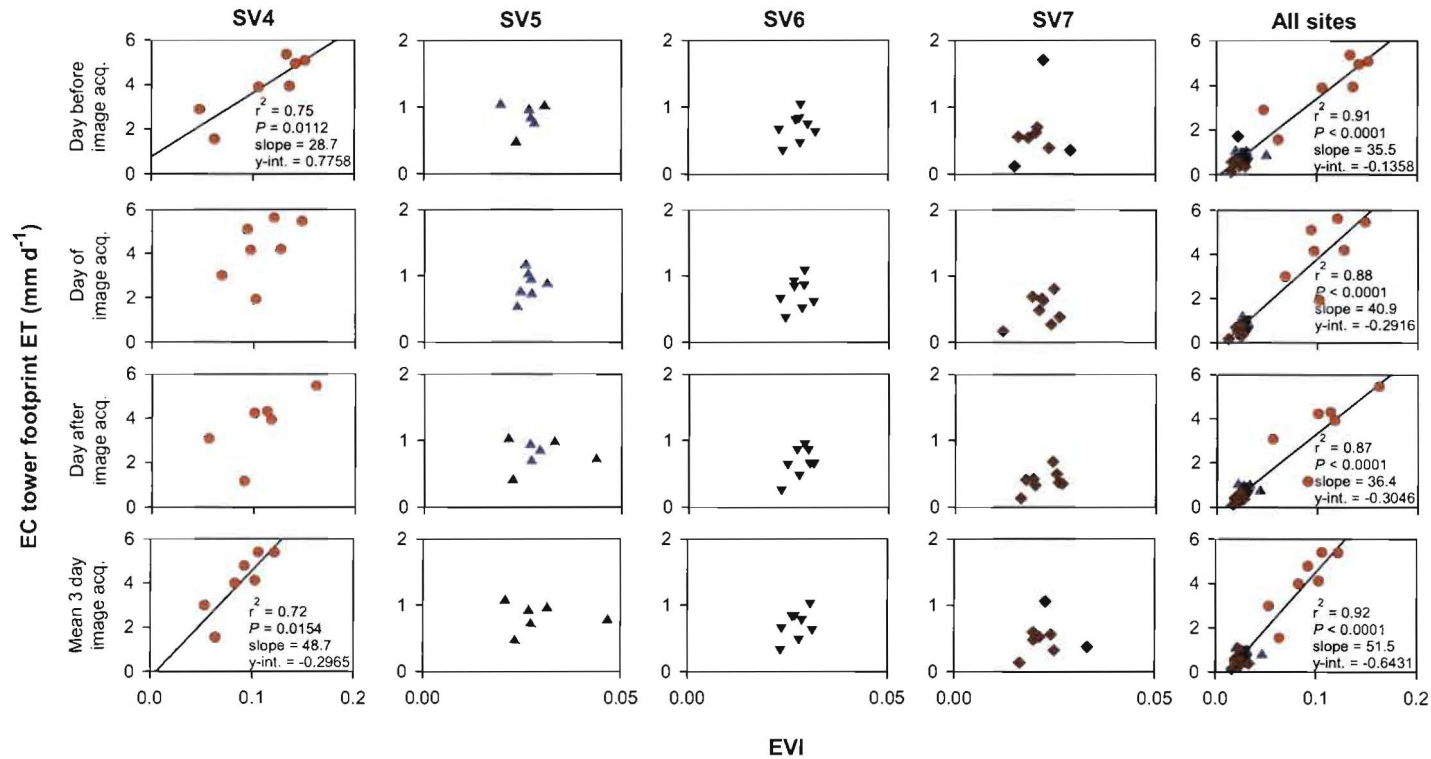
Figure 17. Relationships of daily ET (24-hour total) measured with EC on corresponding daily EVI values calculated for the EC tower footprint of the day before, day of, and day after Landsat TM 5 image acquisition dates for each study site (SV4, SV5, SV6 and SV7). Each point in each panel represents the daily ET and EVI value for each of the nine satellite sampling dates. The row of panels on the far right represents all sites and sampling dates.
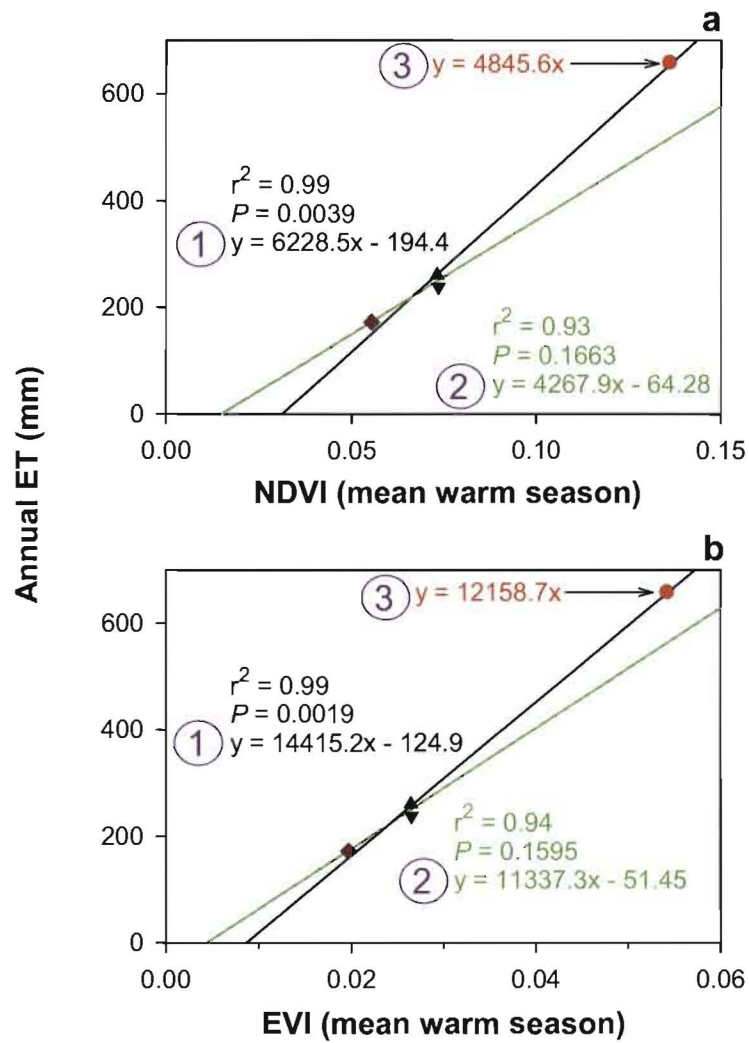
Figure 18. Relationships of mean annual ET on mean growing season NDVI across all four study sites (black line, Regression "1"), across the three shrub sites (green line, Regression "2"), and for the grassland site (SV4; Regression "3") (**a**); and the same for EVI (**b**). Regressions 1-3 were used to extrapolate to whole-basin ET.

(**Fig. 18a, black line**), or on mean warm season EVI (**Fig. 18b, black line**) across all four

sites, were all statistically significant ($P<0.01$) and strong (r^2 values=0.99). Remarkably,

regression relationships for annual ET on mean warm season NDVI (and EVI) calculated

across just the shrub sites were also strong (**Fig. 18**, green lines in each panel). However,

slopes of these regression lines were 20% to 32% as steep as those calculated using data

from all four sites. The frequency distributions of mean annual NDVI and EVI values of

all the 25 x 25 m Landsat TM pixels within the phreatophytic (lowland) area of Spring

Valley in 2007 showed on average 87% (86% for NDVI and 88% for EVI) of all pixels

fell within the range that corresponded to vegetation indices typical of the shrub sites

(**Fig. 9**), with only an average of 13% (14% for NDVI and 12% for EVI) of all pixels in

the valley having vegetation index values at, or above, those corresponding to the

grassland agricultural site (SV4). These results enhanced confidence in using Regression

2 (**Fig.18**) to calculate annual ET for all non-water-covered pixels with NDVI values less

than or equal to 0.13, and EVI values less than or equal to 0.055 (excluding the Yelland

playa - as mapped by SNWA). To calculate annual ET for NDVI and EVI values above

0.13 and 0.055, respectively, Regression 1 (**Fig. 18**) was used, as well as the simple ratio

of annual ET for site SV4 to mean growing season NDVI, or EVI, for that site

(Regression 3, **Fig. 18**).

Addition of abiotic factors to enhance prediction of ET from NDVI/EVI

At individual sites, incorporating abiotic factors (air temperature, PFD, soil temperature,

VPD) in multiple linear regressions that included vegetation indices from all image

acquisition dates improved regression P- and r^2-values somewhat (**Appendix**

Table A2), but this effort did not lead to statistical significance. When data from all sites

were pooled in the analyses (i.e. to include SV4) and the additional abiotic factors were

included significance (*P*-values) and power (r^2 values) of regressions that predict daily

ET improved from 0.83-0.90 to 0.89-0.95 for r^2 values. Thus, including additional factors

in equations already containing a vegetation index was only marginally helpful. The best

predictive relationships between vegetation indices and ET were obtained at longer time

scales, particularly with mean growing season NDVI or EVI, explaining in excess of 90%

of the variability in annual ET (**Fig. 18**). This was true not only when regressions

included all four sites but also when they included only the three shrubland sites (**Fig.

18**).

Temporal patterns in ground water level

Mean depth to ground water differed among sites and ranged from 0.7 m to 4.5 m

below ground surface (**Fig. 19a**) with a seasonal range of water level change of about 200

mm (0.66 ft) (SV4) to 400 mm (1.3 ft) (SV5) across the sites (**Fig. 19b**). The three sites

with native shrub cover showed a similar temporal pattern in ground water level change

during the year. Levels decreased almost linearly and relatively steeply from May to July

(SV7) or August (SV5, SV6) and then declined less steeply until they reached their

lowest levels in early September (SV7) or early October (SV5, SV6), after which they

began to increase. Ground water levels increased linearly at sites SV5 and SV6 through

April 2008, but at a rate almost 30% faster at site SV6 versus site SV5. At site SV7, the

rate of increase in ground water level measured between early September and early

October was similar to the rate observed at site SV5 between early October and mid-

a

b
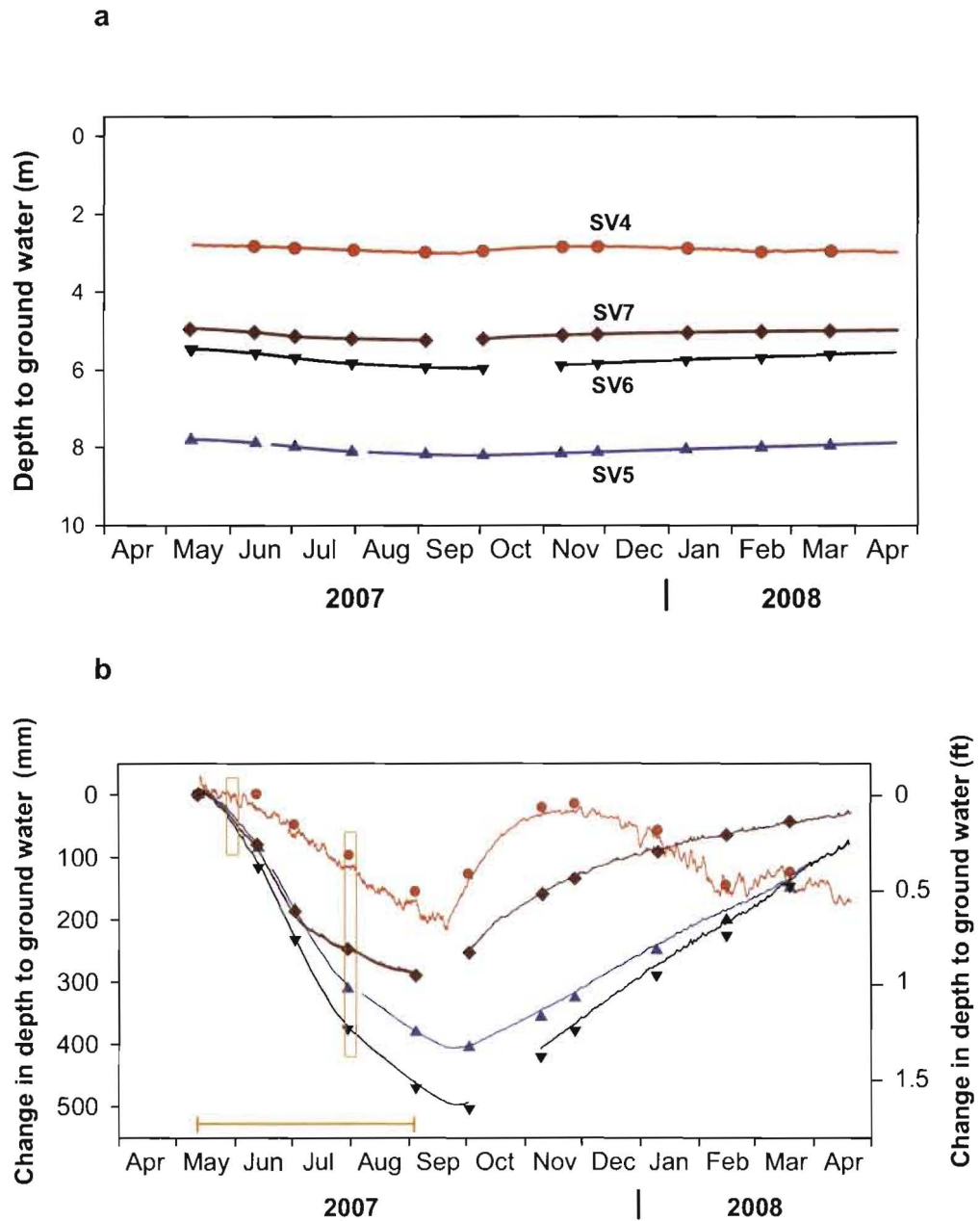
Figure 19. Time courses of (**a**) depth to ground water (meters below surface), and (**b**) changes in depth to ground water, at each of the four sites during the study year. Monitoring wells were located near the EC towers at the study sites. Orange boxes in panel **b** correspond to weekly periods shown in **Figure 20a** and **20b**.

November. Ground water levels at SV7 then increased at a slower and slower rate as

April 2008 was approached. By the end of the study year, ground water levels at all

shrub-covered sites had almost completely recovered to levels observed one year earlier.

At site SV4, ground water level during the summer 2007 dropped at a much slower rate

began to increase. Ground water levels increased linearly at sites SV5 and SV6 through

April 2008, but at a rate almost 30% faster at site SV6 versus site SV5. At site SV7, the

rate of increase in ground water level measured between early September and early

October was similar to the rate observed at site SV5 between early October and mid-

November. Ground water levels at SV7 then increased at a slower and slower rate as

April 2008 was approached. By the end of the study year, ground water levels at all

shrub-covered sites had almost completely recovered to levels observed one year earlier.

At site SV4, ground water level during the summer 2007 dropped at a much slower rate

(35-55% slower) than observed at the other sites, albeit in the same linear fashion, with

no discernable change in the rate until the minimum level was measured on 21 September

2007. Unlike at the other sites, ground water levels at SV4 rose abruptly and rapidly after

this date also at a slower and slower rate until it temporarily reached levels in December

2007 that were very close to those measured at the start of the study. This full recovery of

ground water level was then followed by another parabolic-like decline that extended

until mid-February 2008 when levels generally rose slowly until mid-April 2008.

General patterns of early growing season ground water level decreases observed at all

sites, and the recovery of ground water levels in the later growing season, appeared to

roughly correspond to temporal patterns in vegetation indices (NDVI and EVI).

Vegetation index data are not available after mid-September 2007, but decreases in

NDVI and EVI at some sites (i.e. SV4, SV6, SV7 in **Fig. 11**) occurred at about the same time that ground water levels showed rapid recoveries (**Fig. 19b**).

Diel to multi-day oscillations in ground water levels observed at sites with native shrubs ranged between 0.5 and 4 mm for most of the study period. At site SV4, these oscillations were significantly larger, recorded from 0.5 to 5 mm between late September and late November 2007, and 0.5 to 15 mm from late June to late September 2007, and from late November 2007 to mid-April 2008. In some cases (e.g. at SV7), diurnal oscillations in ground water level appeared to correspond to diurnal oscillations in ET. Diel oscillations in ground water level measured from May to June 2007 (**Fig. 20a**), when vegetation had green leaves, generally did not correspond with daily ET at each of the four sites, although synchronization between ET and ground water level was apparent during the late growing season, especially at SV7 (**Fig. 20b**). Cumulative changes in ground water level paralleled cumulative ET over the same early season observation periods (**Fig. 21**). The slope of the relationship between ground water level and ET showed two distinct linear relationships that corresponded to (1) a period earlier in the growing season where cumulative rate of ground water level decline was relatively steep, and (2) a period later in the growing season when cumulative rate of ground water level decline was less steep (see **Fig. 19b**). This behavior in ground water level over time at each site also corresponded to the date at which the rate of cumulative ground water level decline slowed but the rate of cumulative ET remained constant (**Fig. 21**). The slopes of the curves from the first part of the growing season ranged from 5.7 to 9.6, while those from the later growing season ranged from 2.1 to 2.3 mm. In contrast, the slope at the grassland site remained unchanged and below 1:1 over the growing season (0.5).
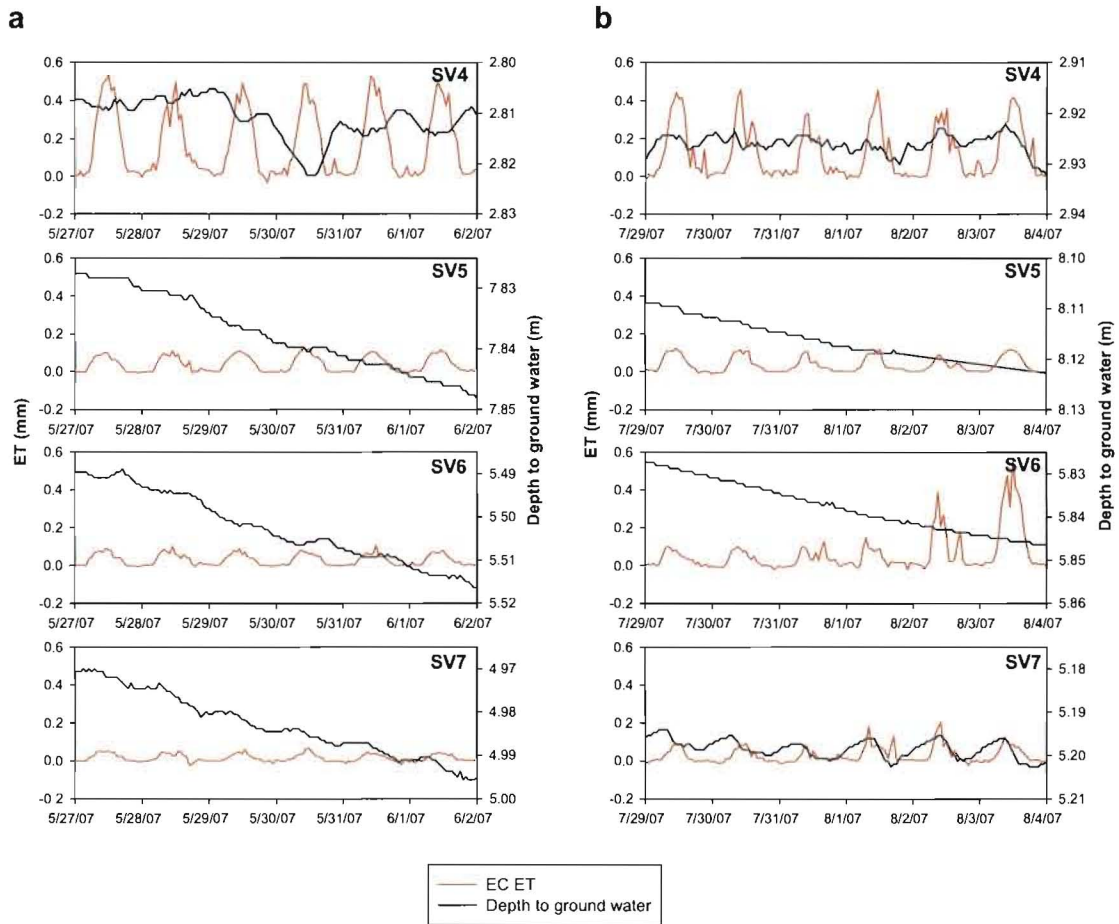
Figure 20. Diel time courses of mean hourly EC ET (red lines, mm per hour) and hourly depth to ground water (black lines, m below surface) over two weekly periods: (**a**) spring 2007; (**b**) summer 2007.
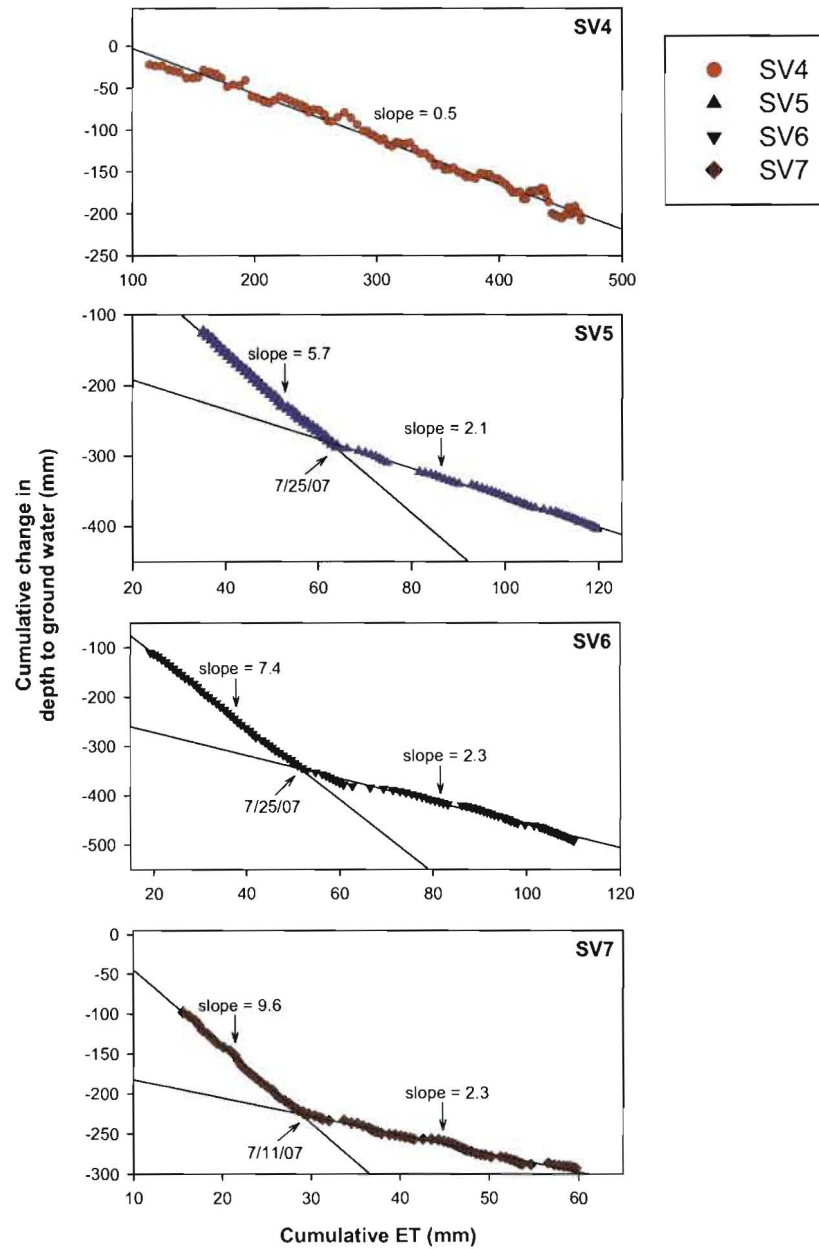
Figure 21. Relationship of cumulative change in ground water levels on corresponding cumulative EC ETs for each of the study sites in Spring Valley for the values within the period of 6 June to 3 September 2007 showing strong linear relationships (simple linear regressions), and changes in slopes at sites SV5, SV6 and SV7, possibly due in part to changes in transpiration by vegetation.

Extrapolation of EC ET to lowland basin-wide ET

Accuracy assessment of equations used to calculate ET (**Table 5**; albeit using "training data" from the four sites) indicate that all extrapolation equations, or combination of regressions, were highly accurate, considering that predicted (modeled) values of annual ET for each site were very close to values measured with EC. However, given the small number of observations (n=4), any assessment of the best regression approach to employ must be viewed cautiously.

Basin-wide ET extrapolations calculated using mean growing season NDVI ranged from about 204,628 to 222,871 acre feet year^{-1} (**Table 6**). Estimates calculated using mean growing season EVI were about 8 to 10% higher. This translated to a difference in basin ET estimates of about 12,000 to 19,000 acre feet year^{-1} when using the two different vegetation indices, excluding error propagations of systematic instrument uncertainty ($\pm$ 5%), satellite measurements, and those associated with extrapolation. Annual basin-wide ET calculated for the study year using the linear regression equation fitted to NDVI data representing all four sites (P_{slope}<0.0039, r^2=0.99; **Fig. 18a**, Regression 1) was nearly identical to basin ET calculated using two regression equations (Regression 2 for the low NDVI sites, NDVI<0.13—P_{slope}=0.17, r^2=0.93; Regression 1 for the high NDVI site, NDVI>0.13). Basin ET calculated using Regressions 2 and 3 in **Figure 18** (Regression 2 for low vegetation index values, Regression 3 for high vegetation index values) produced estimates that were about 8% lower than those calculated using just Regression 1 or a combination of Regressions 1 and 2.

If an average downward correction adjustment of 29%, derived from simultaneous EC ET-to-dome ET measurements, is applied to whole-basin estimates

Table 5. Correspondence of measured annual ET (mm year-1) at each site using EC with annual ET calculated (mm year-1) for that site using the regression protocols (various combinations of regressions "1", "2" and "3") described in the Methods and given in **Figure 18** using mean growing season NDVI (top rows) and mean growing season EVI (lower rows). Statistics for regression equations using data points from all sites together for each of the calculation protocols (under "Predicted ET") for each of the vegetation indices is given below each (NDVI, EVI) site-by-site summary.

Vegetation index	Site	Measured EC ET	Predicted ET		
			Regression ①	Regressions ① & ②	Regressions ② & ③
NDVI	SV4	659	653	635	585
	SV5	260	261	250	249
	SV6	238	264	251	251
	SV7	172	151	192	188
	Relationship of measured on predicted				
	Slope		1.484	1.465	1.255
	P_{slope}		0.004	0.001	0.001
	r^2		0.992	0.997	0.998
	y-intercept		-1.946	-1.093	-6.495
EVI	SV4	659	656	642	604
	SV5	260	257	250	249
	SV6	238	257	250	250
	SV7	172	159	186	184
	Relationship of measured on predicted				
	Slope		0.999	1.057	1.158
	P_{slope}		0.002	0.001	0.001
	r^2		0.996	0.998	0.998
	y-intercept		0.175	1.872	0.998

Table 6. Annual ET (20 April 2007 to 20 April 2008) calculated for the phreatophyte area (open water bodies and Yelland playa (as mapped by SNWA) excluded) in Spring Valley in eastern Nevada using regressions given in **Figure 18** (circled numbers). Data in lower part of table represents basin wide ET data that have been adjusted based on static chamber dome with EC tower comparisons (see **Figs. 13** and **14** dome-EC comparisons, **Table 4**) showing an average downward adjustment of 29% (mean of average site-specific percentage differences from measured EC ET--34, 39, 35 and 8%=29%--and average cross-site percentage difference from measured EC ET--16%, see **Table 4**). Note: The total acres summed from the NDVI-based and EVI-based ET images were 156,446 and 156,477, respectively (31 acres difference in water body detection via negative VI thresholds).

Vegetation index	Extrapolated basin-wide ET (acre feet yr^{-1})		
	Regression ①	Regressions ① & ②	Regressions ② & ③
NDVI	222,871	220,912	204,628
EVI	240,976	240,231	224,942
	Static chamber dome adjusted basin-wide ET (acre feet yr^{-1})		
NDVI	158,238	156,847	145,286
EVI	171,093	170,564	159,709

calculated with Regressions 2 and 3 (**Table 6**), whole-basin ET estimates for the study

year are reduced to 145,286 and 159,709 acre feet year^{-1}, for NDVI and EVI,

respectively.

Discussion

Quantification of ET from EC with and without static chamber adjustments

Unadjusted ET values measured at all sites using EC were comparable to values

estimated/reported using EC for similar sites in other studies in the same and neighboring

valleys in the Great Basin of eastern Nevada (D. Devitt, pers. comm.). The relationship

(**Fig. 14**) between the EC ET rates versus dome ET rates at each of the sites indicates that

both methods recorded parallel changes in ET rates over multiple diel cycles (**Fig. 13**).

Explanations for these differences between the two methods (**Table 4**) are speculative but

may include dome-related issues such as possible modifications of the microclimate

around soils and plants during measurements that may impact transpiration or

evaporation; slight attenuation of PFD (Arnone & Obrist 2003); differences in spatial and

temporal scale between methods; and the introduction of potential errors inherent to the

micrometeorological calculations of latent heat flux using eddy covariance (e.g. Lee *et al.*

2004). We sought to minimize the generation of potential errors when using the static

chamber by sampling at multiple locations within each EC tower footprint; matching

dome measurements to the actual EC tower footprint at the time of measurement; and

adjusting each calculated dome ET rate for a specific percent vegetation and soil cover to

match the average plant canopy cover of the EC tower footprint.

Relatively high annual energy balance closures (94% averaged across sites) calculated for all sites suggest that EC ET estimates are quite robust, especially relative to those measured at other sites or in other ecosystems (Wilson *et al.* 2002). On the other hand, consistently lower ET measured with the dome static chamber, relative to ET derived from EC, seen <u>at</u> all four sites and when viewed <u>across</u> all four sites during the growing season, suggests that actual, or "true", ET may lie somewhere between estimates derived using the two methods. Published comparisons of ET values obtained from concurrent measurements of ET using chambers and eddy covariance are very few but show cases where the two methods agree with each other (Hammerle *et al.* 2007) where chambers estimate higher ET (Stannard & Weltz 2000—post monsoonal conditions; Pickering *et al.* 1993 chamber comparison to lysimeter ET at midday in peanut crops with high leaf area indices) and where chambers estimate lower ET (Steduto *et al.* 2002—chamber vs. lysimeter using artichoke; Arnone *et al.* 2008, this study). Even the calculation of energy balance closure is subject to a level of uncertainty that depends on inherent errors associated with: (a) the calculation of latent and sensible heat fluxes from EC data, as well as the calculation of soil heat flux; and (b) the assumption that net radiation measured at the location of the EC tower represents the entire footprint area sampled by the CSAT sonic anemometer and 7500 open-path IRGA. Thus, careful comparison of simultaneously measured chamber and EC ET data collected in the present study, and qualitative consideration of the potential sources of errors associated with the two methods, leads to the conclusion that the actual, or "true", ET that occurred in the phreatophytic zone of Spring Valley from April 20, 2007 to April 20, 2008 probably lies in the range expressed by the two methods.

Using vegetation indices to predict ET

The poor relationships observed between daily ET and vegetation indices calculated for the specific image acquisition dates (**Fig. 16**, **Fig. 17**) within sites demonstrates the difficulty of using seasonal changes in NDVI and EVI obtained during the growing season to accurately calculate even site-specific total annual ET. Improved regression fits observed between mean growing season vegetation index values and annual ET (**Fig. 18**) appear to buffer smaller spatial and temporal scale variability and ultimately allow for reasonably robust estimat of basin-wide annual ET (Devitt *et al.* 2008, Groeneveld *et al.* 2007). Using site- and date-specific vegetation index and daily ET values to accurately scale to even site-specific annual ETs is extremely difficult and likely cannot be validated.

However, differences observed in the slopes and intercepts of linear regressions fitted to points from all four sites (Regression 1 in **Fig. 18a** and **18b**) and regression lines fitted to just the points representing the low NDVI/EVI shrub sites (Regression 2 in **Fig. 18a** and **18b**) suggest that using a single regression equation that spans the full range of mean growing season NDVI/EVI values may misrepresent the relationship between ET and vegetation indices for low NDVI/EVI areas. Given that the frequency distribution of mean growing season NDVI/EVI values for all pixels within Spring Valley was strongly skewed to the low end of the vegetation index axes (**Fig. 9**), it would seem more accurate to apply the regression equations in one of two ways to calculate basin-wide ET. First, Regression 1 can be applied to all pixels in the phreatophytic basin area with a mean growing season NDVI > 0.13, or EVI value > 0.055, and Regression 2 to all pixels having a NDVI ≤ 0.13, or EVI ≤ 0.055. Or, second, Regression 2 could be applied to

pixels for NDVI ≤ 0.13, or EVI pixels ≤ 0.055, and Regression 3 could be applied to

pixels for NDVI > 0.13, or EVI pixels > 0.055.

Inferring ET from ground water level changes

The use of ground water level changes as another means to estimate site-specific

ET—particularly ground water ET—could not be done with the existing ancillary data,

even though diel patterns in water level and ET at SV7 corresponded with each other

during certain periods in the study year (**Fig. 20**). At the seasonal time scale, the

significant and linear decline in ground water levels observed across all sites generally

corresponded to temporal patterns in a number of covarying biotic (e.g. plant canopy

development and senescence) and abiotic factors (e.g. cumulative solar radiative input

and energy storage in soils from spring through summer, or cumulative net radiative

output from ecosystems from summer to fall to winter). However, deriving a clear causal

explanation for ground water level declines and recoveries is difficult. The unavailability

of ground water pumping records from local ranchers further complicates the

interpretation of seasonal changes observed in ground water levels at all sites, but

especially at the grassland site (SV4).

At the shrub sites, the linear declines in ground water levels correlated with

cumulative ET, and the change in the slope of ground water levels plotted as a function of

cumulative ET (**Fig. 21**) suggests that plant transpiration may account for some of the

change in ground water level over the course of the year, especially if plants acted as

phreatophytes. However, for all shrub sites and times during the growing period, the

amount of water lost via ET, as measured using the EC method, represented only a small

fraction of the amount of ground water change measured, as indicated by slopes of cumulative ground water level on cumulative ET that were two to almost 10 times greater than a 1:1 slope, even accounting for the storage coefficient of the aquifer. At site SV4, cumulative ET water losses exceeded cumulative reductions in ground water level by almost a factor of two, suggesting either that vegetation relied on water stored in the vadose zone to a large degree, or that ground water levels at this site were replenished from upslope surface sources (i.e. mountain front recharge from snowmelt or sprinkler irrigation of upslope fields).

Similarly, at the day-to-day time scale, the daily amount of water evapotranspired at any of the sites appeared to be unrelated to the amount of ground water level change that was measured contemporaneously (**Fig. 22**). Though the results are not conclusive, they suggest that transpiration at sparsely vegetated shrub sites contributed relatively little to overall ET (i.e. soil evaporation dominated) or that ground water levels at the study sites are controlled by other hydrogeologic factors other than the effects of surface vegetation. The results do not indicate, however, that phreatophytic transpiration is not a significant contributor to total ecosystem ET. These data show that partitioning of the water sources into vadose-derived versus ground-water-derived may require additional work, especially with respect to aquifer characterization. A number of researchers (White 1932; Troxell 1936; Gatewood *et al.* 1950; Meyboom 1967; Tromble 1977; Gerla 1992; Rosenberry & Winter 1997; Lewis *et al.*, 2002; Loheide *et al.*, 2005) have shown that monitoring ground water levels could be useful for predicting ground water ET. The more recent cases, however, have pointed to the need to better characterize the hydraulic conductivity and storage coefficient of the aquifer, as these are major factors influencing
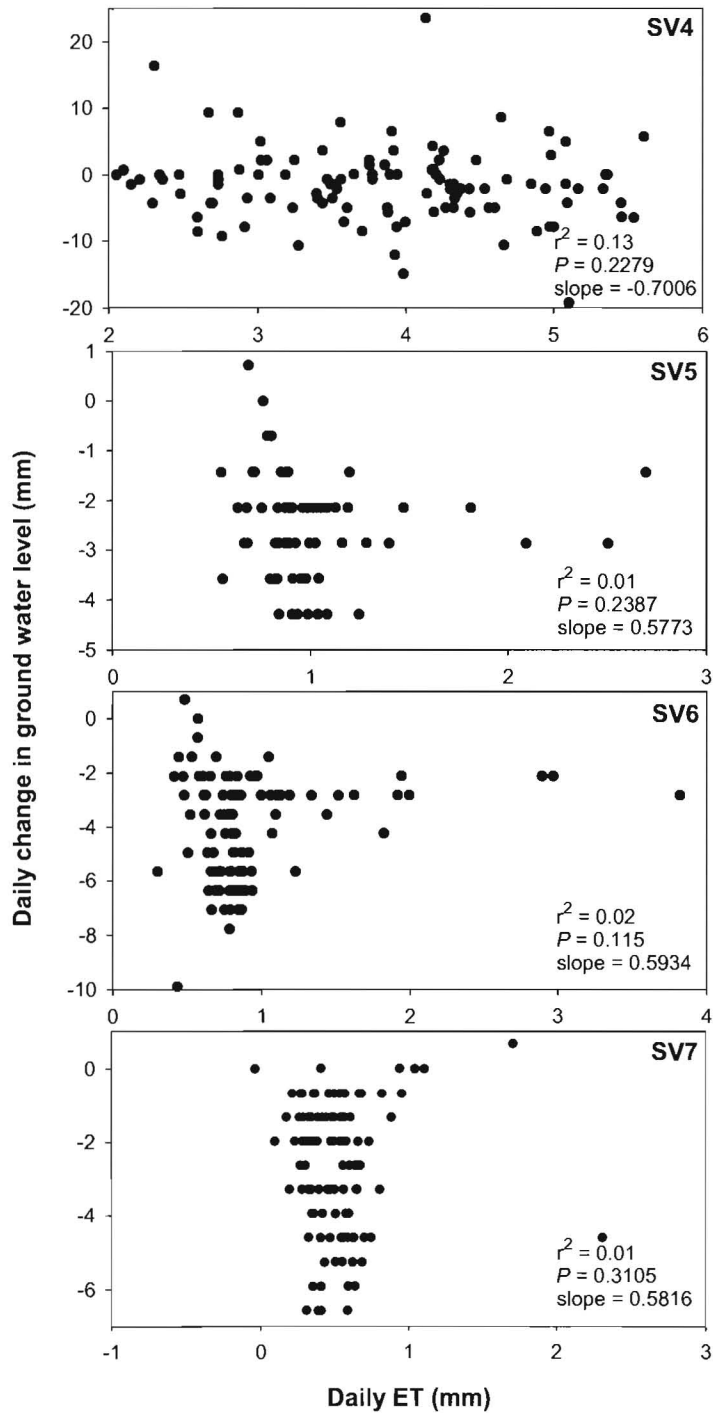
Figure 22. Relationship of daily change in ground water level on daily ET for each of the study sites in Spring Valley.

the degree of the ground water fluctuation given plant uptake. Our results, which did not show good predictability, should be considered a first attempt at using ground water fluctuations, because major efforts were not taken to characterize the aquifers. In any case, the results point to the need for better accounting of all ecosystem hydrologic flows and pools including the amount and timing of ground water pumping, and the quantification of other sources of ground water (i.e. mountain front recharge, spring recharge, etc.).

Variability in basin-wide ET estimates

The absence of large differences in whole-basin ET estimates (**Table 6**) derived from the three different regression protocols (**Fig. 18** and **Table 5**) suggests a robustness in the relationship between ET and vegetation indices at large, integrative temporal scales (e.g. annual ET, mean growing season vegetation index values) that were not seen at shorter (monthly) time scales, and at smaller scales approaching individual sites. However, the apparent similarity in the validity (accuracy) of the regression approaches should not be the only criterion used to decide which approach to apply when extrapolating site-level ET rates to the annual basin-wide ET volumes. Two other observations from our data should be considered.

First, clear differences in the slopes of the regression lines passing through the low NDVI/EVI site data points (**Fig. 18a, 18b**) were observed when compared to the lines passing through all four points, and when compared to the ratios of annual ET to mean NDVI (or mean EVI) for site SV4, with the high ET/high NDVI/EVI values. This result suggests the need for separate extrapolation equations for low and high NDVI/EVI

pixels, e.g. for water limited versus non-water limited areas. Second the highly skewed distribution of total basin pixels (87%) with low mean growing season NDVI/EVI values versus the relatively few pixels with higher NDVI/EVI values (**Fig. 9**) also suggests separate treatment of low and high NDVI/EVI pixels. Certainly, as additional EC ET, dome ET, environmental, and imagery data are collected and acquired in this valley, through extension of measurements at existing ET towers or as new EC towers are added to the monitoring network, the extrapolated basin-wide ET values can be more robustly assessed. Existing datasets from this valley should also be used to assess the accuracy of our ET estimates and increase confidence in ground water discharge through ET.

Conclusions

Together, results from this one-year study provide some new quantitative estimates of site-specific and basin-wide ET that should help improve the accuracy of estimating ET from Spring Valley. Because our study focused on the measurement of total ET, a quantitative estimate of ground water ET, or phreatophytic transpiration, was not possible. An average of 94% energy balance closure calculated across all sites in the present study using EC data also suggests that half-hourly ET values from Spring Valley provide better-than-average confidence (see Wilson *et al.* 2002) in the accuracy of ET estimates. However, significantly lower ET estimates calculated using the large static chamber, compared to simultaneous estimates of EC ET measured during the growing season, and qualitative consideration of the potential sources of errors associated with the two methods, suggest that the actual, or "true", ET that occurred in the phreatophytic zone of Spring Valley from April 20, 2007 to April 20, 2008 probably lies in the range

expressed by the two methods. Finally, the best estimates of basin-wide ET are likely provided by the application of linear regression equations of mean annual growing season NDVI, or EVI, on total annual ET that predict annual ET for each Landsat 5 TM pixel. However, separate regression equations should be applied to low and high NDVI/EVI pixels, respectively; one regression equation developed for low NDVI/EVI pixels and another regression equation developed for high NDVI/EVI pixels.

Limitations

To quantitatively measure the phreatophytic contribution to total ET, which is more reflective of actual ground water use by plants/vegetation, a more comprehensive analysis that includes isotopic examination (e.g. ^{18}O in soil, plant and ground water) would be extremely powerful (e.g. similar to those done in earlier studies: Yakir *et al.* 1990; Dawson & Ehleringer 1991; Brunel *et al.* 1995; Obrist *et al.* 2004; Chimner & Cooper 2004). This would provide direct measurement of plant water source from either ground water or vadose zone water. Other measurements to narrow down components of the water budget would also enhance the accuracy of ET estimates. These would include measurements of soil water content in the vadose zone, the amount and timing of plant water uptake via automated and logged direct sapflow measurements (e.g. Pataki *et al.* 2000) and leaf stomatal activity in concert with EC and dome ET measurements. Continuous monitoring of plant canopy development, both duration and senescence (e.g. satellite accessible web cameras or ground-based NDVI sensors) would also correlate ET rates to actual plant activity.

Significantly lower ET estimates calculated using the large static chamber, compared to simultaneous estimates of ET measured during the growing season, point to the need for more comprehensive comparison of the two methods used to quantify ET. Thus, the causes of discrepancies observed in this study between the two methods should be investigated more fully across additional landscapes and sites over longer time periods under varying moisture conditions.

Further, the validity and accuracy of relatively simple, satellite-derived vegetation indices to extrapolate EC ET or dome ET estimates to entire basins need to be re-examined. The results here showed that significant improvements in extrapolation potential requires that temporal and spatial variabilities be accounted for, especially when the relationship is used to predict ET rates for different canopies and vegetation coverage. Concerted effort should thus aim at sorting out confounding non-vegetation contamination of Landsat TM images that derive from the presence of water on or within near-surface soils, low sun angle in winter months, the presence of snow on soil and vegetation, and, the presence of clouds. Moreover, the efforts should include the use of other satellite based land and vegetation data (e.g. high spatial resolution IKONOS multispectral imagery) to complement NDVI and EVI remotely sensed data derived from Landsat TM.

Finally, the sizeable range of ET estimates presented for the single year of our study suggest that continuing ET measurements using multiple measurement and extrapolation methods, along with some additional techniques, would significantly enhance future estimates of total and phreatophytic ET. With additional research efforts

focused on resolving the issues outlined here, the robustness and science-based reliability

of management decisions will be enhanced.

References

Allen, V.G., C.P. Brown, R. Kellison, E. Segarra, T. Wheeler, P.A. Dotray, J.C.

Conkwright, C.J. Green, V. Acosta-Martinez (2005), Integrating cotton and beef

production to reduce water withdrawal from the Ogallala aquifer in the southern

high plains, *Agronomy Journal*, 97, 556-567.

Allen, V.G., C.P. Brown, E. Segarra , C.J. Green, T.A. Wheeler, V. Acosta-Martinez,

T.M. Zobeck (2008), In search of sustainable agricultural systems for the Llano

Estacado of the US Southern High Plains, *Agriculture Ecosystems and

Environment*, 14, 3-12.

Arnone, J.A. III, D. Obrist (2003), A large daylight geodesic dome for the quantification

of whole-ecosystem CO_2 and water vapour fluxes in arid shrublands, *Journal of

Arid Environments*, 55, 629-643.

Aubinet, M., A. Grelle, A. Ibrom *et al.* (2000), Estimates of the annual net carbon and

water exchange of forest: the EUROFLUX methodology, *Advances in Ecological

Research*, 30, 113-175.

Aubinet, M., B. Chermanne, M. Vandenhaute, B. Longdoz , M. Yernaux , and E. Laitat

(2001), Long term carbon dioxide exchange above a mixed forest in the Belgian

Ardennes, *Agricultural and Forest Meteorology*, 108, 293-315.

Baldocchi, D.D. (2003), Assessing the eddy covariance technique for evaluating carbon

dioxide exchange rates of ecosystems: past, present and future, *Global Change

Biology*, 9, 479-492.

Baldocchi, D.D., E. Falge, L. Gu *et al.* (2001), FLUXNET: A new tool to study the

temporal and spatial variability of ecosystem-scale carbon dioxide, water vapor

and energy flux densities, *Bulletin of the American Meteorological Society*, 82,

2415-2435.

Brunel, J.P., G.R. Walker, A.K. Kennett-Smith (1995), Field validation of isotopic

procedures for determining source water used by plants in a semi-arid

environment. *Journal of Hydrology*, 167, 351-368.

Cablk, M.E., C. Kratt (2007), A methodology for mapping shrub canopy in the Great

basin using high spatial resolution satellite imagery, *Desert Research Institute

Publication*, #41236.

Chander, G., B. Markham (2003), Revised Landsat-5 TM radiometric calibration

procedures and postcalibration dynamic ranges, *IEEE Transactions on

Geoscience and Remote Sensing*, 41, 2674-2677.

Chimner, R.A., D.J. Cooper (2004), Using stable oxygen isotopes to quantify the water

source used for transpiration by native shrubs in the San Luis Valley, Colorado,

USA, *Plant and Soil*, 260, 225-236.

Committee on the scientific basis of the Colorado basin water management (2007),

Colorado River basin management: Evaluating and adjusting to hydroclimate

variability, 1-222.

Dawson, T.E, J.R. Ehleringer (1991), Streamside trees that do not use streamwater, *Nature*, 350, 335-337.

Denmead, O.T., F.X. Dunin, S.C. Wong, E.A.N. Greenwood (1993), Measuring water use efficiency of Eucalypt trees with chambers and micrometeorological techniques, *Journal of Hydrology*, 150, 649-664.

Devitt, D., L. Fenstermaker, M. Young, B. Conrad, M. Baghzouz, B. Bird (2008), Evapotranspiration Estimates in North Eastern Nevada Basins, *Draft Report to the Southern Nevada Water Authority.*

Dugas, W.A., D.C. Reicosky, J.R. Kiniry (1997), Chamber and micrometeorological measurements of CO_2 an H_2O fluxes for three C4 grasses, *Agricultural and Forest Meteorology*, 83, 113-133.

EROS, (2006), http://eros.usgs.gov/products/satellite/tm.html#search.

Farrand, W.H., R.B. Singer, and E. Merényi (1994), Retrieval of apparent surface reflectance from AVIRIS data: a comparison of empirical line, radiative transfer and spectral mixture methods, *Remote Sensing of the Environment*, 47, 311-321.

Flerchinger, G.N., C.L. Hanson, J.R. Wight (1996), Modeling evapotranspiration and surface energy budgets across a watershed, *Water Resources Research*, 32, 2539-2548.

Foken, Th., B. Wichura (1996), Tools for quality assessment of surface-based flux measurements, *Agricultural and Forest Meteorology*, 78, 83-105.

Foken, Th., M. Göckede, M. Mauder, L. Mahrt, B. Amiro, W. Munger (2004), Post-field data quality control, *Handbook of Micrometeorology* (eds Lee, X., W. Massman, B. Law), 181-208.

Gash, J.H.C., A.J. Dolman (2003), Sonic anemometer (co)sine response and flux

measurement I. potential for (co)sine error to affect sonic anemometer-based flux

measurements, *Agricultural and Forest Meteorology*, 119, 195–207.

Gatewood, J.S., T.W. Robinson, B.R. Colby, J.D. Hem, L.C. Halpenny (1950), Use of

water by bottom-land vegetation in lower Safford Valley, Arizona, *U.S.*

Geological Survey Water Supply Paper, 1103.

Gee, G, D. Or. (2002), Particle-Size Analysis, *in* Methods of Soil Analysis, Part 4

Physical Methods, J. Dane and C. Topp, editors. Soil Science Society of America

Book Series, vol. 5.

Geissbühler, P., R. Siegwolf, W. Eugster (2000), Eddy covariance measurements on

mountain slopes: the advantage of surface-normal sensor orientation over a

vertical set-up, *Boundary-Layer Meteorology*, 96, 317–392.

Gerla, P.J. (1992), The relationship of water table changes to the capillary fringe,

evapotranspiration, and precipitation in intermittent wetlands, *Wetlands*, 12, 91-

98.

Glenn, E.P., A.R. Huete, P.L. Nagler, K.K. Hirschboeck, P.Brown (2007) Integrating

remote sensing and ground methods to estimate evapotranspiration, *Critical*

Reviews in Plant Sciences, 26, 139-168.

Groeneveld, D.P., W.M. Baugh, J.S. Sanderson, D.J. Cooper (2007), Annual ground

water evapotranspiration mapped from single satellite scenes, *Journal of*

Hydrology, 344, 146-156.

Ham, J.M., J.L. Heilman (2003), Experimental test of density and energy-balance corrections on carbon dioxide flux as measured using open-path eddy covariance, *Agronomy Journal*, 95, 1393-1403.

Hammerle, A., A. Halwanter, M. Schmitt, M. Bahn, U. Tappeiner, A. Cernusca, G. Wohlfahrt (2007), Eddy covariance measurements of carbon dioxide, latent and sensible energy fluxes above a meadow on a mountain slope. *Boundary Layer Meteorology*, 122, 397-416.

Hastings, S.J., W.C. Oechel, A. Muhlia-Melo (2005), Diurnal, seasonal and annual variation in the net ecosystem CO_2 exchange of a desert shrub community (Sarcocaulescent) in Baja California, Mexico, *Global Change Biology*, 11, 927-939.

Hatton, T., R. Evans, S. Knight Merz (1998), Dependence of ecosystems on ground water and its significance to Australia, Occasional Paper 12/98, *Land and Water Research and Development Corporation*, Canberra, Australia, 77.

Heijmans, M.M., P.D., W.J. Arp, F.S. Chaplin III (2004), Carbon dioxide and water vapour exchange from understory species in boreal forest, *Agricultural and Forest Meteorology,* 123, 135–147.

Hsieh, C.I., G. Katul, T.W. Chi (2000), An approximate analytical model for footprint estimation of scalar fluxes in thermally stratified atmospheric flows, *Advances in Water Resources*, 23, 765-772.

Huete, A., K. Didan, T. Miura, E.P. Rodriguez, X. Gao and L.G. Ferreira (2002), Overview of the radiometric and biophysical performance of the MODIS vegetation indices, *Remote Sensing of Environment,* 83, 195–213.

Jasoni, R.L., S.D. Smith, and J.A. Arnone III (2005), Net ecosystem CO_2 exchange in

    Mojave Desert shrublands during the eighth year of exposure to elevated CO_2,

    Global Change Biology, 11, 749-756.

Jury, W.A., H.J. Vaux (2007), The emerging global water crisis" managing scarcity and

    conflict between water users, *Advances in Agronomy*, 95, 1-76.

Kaimal, J.C., J.J. Finnigan (1994), Atmospheric boundary layer flows: Their structure

    and measurement. *Oxford University Press*, New York, NY, pp. 289.

Le Maitre, D.C., D.F. Scott, C. Colvin (1999), A review of information on interactions

    between vegetation and ground water, *Water SA*, 25, 137-152.

Lee, X., J. Finnigan, K.T Paw U (2004), Coordinate systems and flux bias error,

    Handbook of Micrometeorology (eds Lee, X., W. Massman, B. Law), 33-66.

Lewis, K., D. Hathaway, H. Shafike (2002), Evapotranspiration-driven diurnal

    fluctuations in ground water levels at San Marcial, New Mexico, in Ground

    Water/Surface Water Interactions, AWRA 2002 Summer Specialty Conference

    Proceedings, edited by J.F. Kenny, *Am. Water Resources Association*, 115-119.

Loescher, H.W., T. Ocheltree, B. Tanner *et al.* (2005), Comparison of temperature and

    wind statistics in contrasting environments among different sonic anemometer-

    thermometers, *Agricultural and Forest Meteorology*, 133, 119-139.

Loheide II, S.P., J.J. Butler, and S.M. Gorelick (2005), Use of diurnal watertable

    fluctuations to estimate ground water consumption by phreatophytes: A saturated-

    unsaturated flow assessment, *Water Resources Research*, 41, W07030.

Massman, W.J. (2000), A simple method for estimating frequency response corrections

    for eddy covariance systems, *Agricultural and Forest Meteorology*, 104, 185-198.

Massman, W.J. (2001), Reply to comment by Rannik on "A simple method for estimating frequency response corrections for eddy covariance systems", *Agricultural and Forest Meteorology*, 107, 247-251.

Massman, W.J., R. Clement (2004), Uncertainty in eddy covariance flux estimates resulting from spectral attenuation, *Handbook of Micrometeorology* (eds Lee X, Massman W, Law B), 67-100.

Meyboom, P. (1967), Ground water studies in the Assiniboine River drainage basin-part II: Hydrologic characteristics of phreatophytic vegetation n south-central Saskatchewan, *Bulletin Geological Survey Canada*, 139.

Nagler, P., J. Cleverly, E. Glenn, D. Lampkin, A. Huete, Z. Wan (2005), Predicting riparian evapotranspiration from MODIS vegetation indices and meteorological data, *Remote Sensing of the Environment*, 94, 17-30.

Nagler, P.L, E.P. Glenn, H. Kim, W. Emmerich, R.L. Scott, T.E. Huxman, A.R. Huete. (2007), Relationship between evapotranspiration and precipitation pulses in a semiarid rangeland estimated by moisture flux towers and MODIS vegetation indices, *Journal of Arid Environments,* 70, 443-462.

Naumburg, E., R. Mata-Gonzalez, R.G. Hunter, T. McLendon, and D.W. Martin (2005), Phreatophytic vegetation and ground water fluctuations: A review of current research and application of ecosystem response modeling with an emphasis on Great Basin vegetation, *Environmental Management*, 35, 726-740.

Nichols, W.D. (1993), Estimating discharge of shallow ground water by transpiration from greasewood in the northern Great Basin, *Water Resources Research*, 29, 2771-2778.

Nichols, W.D. (1994), Ground water discharge by phreatophytic shrubs in the Great

    Basin as related to depth to ground water, *Water Resources Research*, 30, 3265-

    3274.

Norwood, C.A. (2000), Water use and yield of limited-irrigated and dryland corn, *Soil*

    Science Society of America Journal, 64, 365-370.

Obrist, D., E.A. DeLucia, J.A. Arnone III (2003), Consequences of wildfire on ecosystem

    CO_2 and water vapor fluxes in the Great Basin, *Global Change Biology*, 9, 563-

    574.

Obrist, D., D. Yakir, J.A. Arnone III (2004), Temporal and spatial patterns of soil water

    following wildfire-induced changes in plant communities in the Great Basin,

    Plant and Soil, 262, 1-12.

Pataki, D.E., R. Oren, W.K. Smith (2000), Sap flux of co-occurring species in a western

    subalpine forest during seasonal soil drought, *Ecology*, 81, 2557–2566.

Pickering, N.B., J.W. Jones, K.J. Boote (1993), Evaluation of the portable chamber

    technique for measuring canopy gas-exchange by crops, *Agricultural and Forest*

    Meteorology, 63, 239-254.

Prater, M.R., D. Obrist, J.A. Arnone III, E.H. Delucia (2006), Net carbon exchange and

    evapotranspiration in post-fire and intact sagebrush communities in the Great

    Basin, *Oecologia*, 146, 595-607.

Puigdefábregas, J., T. Mendizabal (1998), Perspectives on desertification: Western

    Mediterranean, *Journal of Arid Environments*, 39, 209-224.

Robinson, T.W. (1958), Phreatophytes, *U.S. Geological Survey Water Supply Paper*,

    1423.

Rosenberry, D.O., T.C. Winter (1997), Dynamics of water table fluctuations in an upland between two prairie-pothole wetlands in North Dakota, *Journal of Hydrology*, 19, 266-289.

Rouse, J.W., R.W. Haas, J.A. Schell, D.W. Deering, J.C. Harlan (1974), Monitoring the vernal advancement and retrogradation (greenware effect) of natural vegetation, Greenbelt, MD, USA, *NASA/GSFCT*, Type 3, Final Report.

Smith, G.M., E.J. Milton (1999), The use of empirical line method to calibrate remotely sensed data to reflectance, *International Journal of Remote Sensing*, 20, 2653-2662.

Stannard, D.I., M.A. Weltz (2006), Partitioning evapotranspiration in sparsely vegetated rangeland using a portable chamber, *Water Resources Research*, 42, W02413.

Steduto, P., Ö. Çetinkökü, R. Albrizio, R. Kanber (2002), Automated closed-system canopy-chamber for continuous field-crop monitoring of CO_2 and H_2O fluxes, *Agricultural and Forest Meteorology*, 111:171-186.

Tromble, J.M. (1977), Water requirements for mesquite (*Prosopis juliflora*), *Journal of Hydrology*, 34, 171-179.

Troxell, H.C. (1936), The diurnal fluctuation in the ground-water and flow of the Santa Ana river and its meaning, *Eos, Transactions, American Geophysical Union*, 17, 496-504.

Tucker, C.J. (1979), Red and photographic infrared linear combinations for monitoring vegetation, *Remote Sensing of the Environment*, 8, 127–150.

Webb, E.K., G.I. Pearman, R. Leuning (1980), Correction of flux measurements for density effects due to heat and water vapour transfer, *Quarterly Journal of the Royal Meteorological Society*, 106, 85-100.

White, W.N. (1932), A method of estimating ground-water supplies based on discharge by plants and evaporation from soil: Results of investigation in Escalante Valley, Utah, *U.S. Geological Survey Water Supply Paper*, 659-A, 1-105.

Wilson, K.B., A.H. Goldstein, E. Falge, M. Aubinet, D. Baldocchi, P. Berbigier, Ch. Bernhofer, R. Ceulemans, H. Dolman, C. Field, A. Grelle, B. Law, T. Meyers, J. Moncrieff, R. Monson, W. Ochel, J Tenhunen R. Valentini, S. Verma (2002), Energy balance closure at FLUXNET sites, *Agricultural and Forest Meteorology*, 113, 223-243.

Wohlfahrt, G., C. Anfang, M. Bahn *et al.* (2005), Quantifying nighttime ecosystem respiration of a meadow using eddy covariance, chambers and modeling, *Agricultural and Forest Meteorology*, 128, 141-162.

Wohlfahrt, G., J.A. Arnone III, L.F. Fenstermaker (2008), Large annual net ecosystem CO_2 uptake of a Mojave Desert ecosystem, *Global Change Biology*, In press.

Yakir D., M.J. DeNiro, J.R.Gat (1990), Natural deuterium and oxygen-18 enrichment in leaf water of cotton plants grown under wet and dry conditions: evidence for water compartmentation and its dynamics, *Plant, Cell and Environment*, 13, 49–56.

Young, M.H., P.J. Wierenga, C.F. Mancino (1996), Large weighing lysimeters for water use and deep percolation studies, *Soil Science*, 161, 491-501.

Zhu, Y., Y. Wua, S. Drake (2004), A Survey: Obstacles and strategies for the

development of ground-water resources in arid inland river basins of western

China, *Journal of Arid Environments*, 59, 351-367.

Acknowledgements

Appendix

Table A1. Average 2007 growing season NDVI and EVI values calculated for the annual EC tower footprints in Spring Valley, Nevada. Site SV4, the agricultural grassland site had the largest values and SV7, the most sparsely vegetated site, had the lowest values.

Site	NDVI	EVI
SV4	0.136	0.054
SV5	0.073	0.027
SV6	0.074	0.027
SV7	0.055	0.020

Table A2. Multiple stepwise regression analysis coefficients (r^2 values) calcualted using mean daily air temperature, soil temperature, PAR, and VPD values in addition to NDVI and EVI, to predict total daily ET using data from all sies and image acquisition dates.

Variable(s)	Day before image acq. r^2	Day of image acq. r^2	Day after image acq. r^2	Mean 3 day image acq. r^2
NDVI	0.90	0.86	0.87	0.91
NDVI + Air T	0.92	0.89	0.91	0.94
NDVI + Air T + Soil T	0.93	0.90	0.91	0.95
NDVI + Air T + Soil T + PAR	0.93	0.92	0.93	0.95
NDVI + Air T + Soil T + PAR + VPD	0.95	0.92	0.93	0.96
EVI	0.90	0.88	0.87	0.92
EVI + Air T	0.92	0.89	0.90	0.92
EVI + Air T + Soil T	0.93	0.91	0.91	0.94
EVI + Air T + Soil T + PAR	0.93	0.92	0.93	0.94
EVI + Air T + Soil T + PAR + VPD	0.95	0.92	0.94	0.95

Depth (ft)	Lithological Description (from cores)
0-2	Brown silt, roots, few large clasts, moist at 2 ft.
5-7	Grey clayey silt, few clasts, roots, dark brown mottling transition to moist soft grey clay, minor clasts, rootS, Fe stainings
10-12	Sand and coarse gravel mixed with fine sand; 11.5 ft. gravel, core loss due to gravel - W.L. - 11.4 ft. bls.
12-13	Large black cobbles (hard) with brown clay matrix
15-17	Brown silty clay, Fe stained mottles, dark brown to black mottling grades into coarse gravel at 16.5 ft., gravel mixed with clay
20-22	Minimal recovery; grey silt to fine sand, Fe staining (sand and gravel - 20.3 to 22ft.)
23-25	Light grey uniform fine sand, well sorted, wet, higher clay content in upper part of core with light colored mottles - W.L. - 19.2 ft. bls.
25	Total Depth - TD

Figure A1. Diagram showing the construction and development of the ground water monitoring well at SV4.

Depth(ft)	Lithological Description (from cores)
0-2	Dry yellow rown silt, roots, uniform grain size
3-5	Coarse sand and gravel, sand at 3.5 ft
5-7	Light brown silt mixed with gravel, gravel lense visable in core at 6 ft.
7-8	Sand and coarse gravel, well rounded, well sorted, dry
10-12	Hard silt and clay, some caliche, light brown in color, some pores blocky texture, dry and friable
15-17	Light brown silt, few roots, dark and light linings, pores; grades into light brown silt sand and gravel grading further into hard silt with white linings
20-22	Yellow brown fine sand uniform size and well sorted, minor clay fraction grading to yellow borwn fine sand, well sorted grades into dry gravel lense
25-27	Hard drilling, 25 to 25.3 ft. - coarse gravel grading into tight light brown clay with mottles - stiff, no water, uniform density
30-32	Soft light brown clay, very moist followed by soft light brown silty clay with minor sand and gravel lenses. Fe stains mottles
35-37	Light brown fine sand, wet, high clay content; gravel at 35.5 ft. followed by light grey fine sand with light grey mottles - water
38-40	Brown fine sand (sediment from drilling). Core mixed coarse sand and gravel at 39 ft., high clay content
40	Total Depth - TD

Figure A2. Diagram showing the construction and development of the ground water monitoring well at SV5.

Depth(ft)	Lithological Description (from cores)
0-2	Soft light brown fine fine and silt at surface followed by dry friable light brown silt to clay, roots, Fe mottling
5-7	Hard orange-red silty clay, mottled transition to red-brown with black stains, roots, small white fragments, moist
10-12	Brown silt, very friable, contains voids, Fe stains, roots followed by light brown to white silt to fine sand, mottled
14-15	Reddish Brown clay, moist, minor amount is coarse sand
15-17	Light reddish brown sand lense at 15 to 15.5 ft. coarse CaCO3 concretions followed by massive moist reddish brown silty clay at 16.5 to 17 ft.
20-22	Reddish brown silty clay, black carbon fragments, vesicular, blocky slightly moist, minor cemented fragments
25-27	Hard blocky fragemnts of cemented clay matrix, followed by coarse sand to gravel light brown in color,v. angular, moist, 26-27 ft. wet clayey silt, no structures - water 18.5 ft.
28-30	Reddish brown fine sand with minor amount of clay becoming enriched in clay in the upper half of core
30	Total Depth - TD

Figure A3. Diagram showing the construction and development of the ground water monitoring well at SV6.

Depth(ft)	Lithological Description (from cores)
0-2	Light brown sand and silt, uniform size, roots; at 3 ft. light greenish grey clay
5-7	Light greenish grey clay, massive, no structures
10-12	Light brown silt changing to grey green silt with minor amount of clay, Fe stains, massive, no structures
15-17	Light green grey clay, some roots, good silt fraction, very moist at 15.6 ft., minor rock fragments
20-22	Light grey clay, very moist, blocky structure, minor amount of silt
23-25	Grey silty clay, roots, no structure grades to silt rich zone in lower part of core
28-29	Smooth and rapid drilling, cutting turning up soupy clay
30-32	Grey silty clay, roots, no structure grades to silt rich zone in lower part of core
33.5	Total Depth - TD

Figure A4. Diagram showing the construction and development of the ground water monitoring well at SV7.

Well Construction Details and General Lithological Descriptions

Spring Valley Area, White Pine County - East of Ely, Nevada
Driller: Andresen Exploration Drilling of Reno, Nevada

Observation Well - SV4

Well Location: NAD 27 – N38.84824, W114.40308
Tower Location: NAD 27 – N38.84821, W114.40314
Elevation: 5807 ft.
Drilled Depth: 25 feet bls.
Borehole Diameter: Augers 7.25-inch
Casing and Screen Size and Material, Wall Schedule, Joint Connection:
                    2-inch PVC, Schedule 40, Flush Joint
Screen Length/Slot Size: Nominal 15 feet/20 slot
Screen Interval from Top of Casing (TOC) – 9.54 ft. to 23.71 ft. w/ 6-inch well point
TOC = grade
Gravel Pack Interval (bls.): 7.25 ft. to 25ft.
Bentonite Hole Plug Interval (hydrated)(bls.): 4.25 ft. to 7.25 ft.
Neat Cement Grout Interval (bls.): 0 ft. to 4.25 ft.
Well Head Completion: Surface Mount Well Vault
Well Development: Inertial water removal, lower water level and monitored recovery
Static Water Level before Development (TOC): 8.21ft.

Split Spoon/Cored Intervals (ft bls.): 0-2, 5-7, 10-12, 15-17, 20-22, 23-25
Recovery respectively (Inches/ 2-ft): 18, 22, 11, 10, 4, and 24

Lithological Description (primarily based on cores) and Depth in feet (bls.):

Depth (ft. bls.)	Description
0-2	Brown silt with roots
5-7	Grey clayey silt transition to soft grey clay with roots
10-12	Sand and coarse gravel w fine sand
12-13	Large cobbles (hard)
15-17	Brown silty clay coarse gravel at 16.5 ft.
20-22	Min. recovery: grey silt to fine sand (sand and gravel-20ft.-22ft.)
23-25	Fine light grey sand, higher clay content in upper core
25	TD

TOC = top of casing
bls. = below land surface

Observation Well - SV5

Well Location: NAD 27 – N39.03232, W114.48481
Tower Location: NAD 27 – N39.03261, W114.48486
Elevation: 5770 ft.
Drilled Depth: 40 feet bls.
Borehole Diameter: Augers 7.25-inch
Casing and Screen Size and Material, Wall Schedule, Joint Connection:
     2-inch PVC, Schedule 40, Flush Joint
Screen Length/Slot Size: Nominal 15 feet/20 slot
Screen Interval from Top of Casing (TOC) – 24.63 ft. to 38.83 ft. w/ 6-inch well point
TOC = grade
Gravel Pack Interval (bls.): 17 ft. to 40 ft.
Bentonite Hole Plug Interval (hydrated) (bls.): 14.50 ft. to 17ft.
Neat Cement Grout Interval (bls.): 0 ft. to 14.50 ft.
Well Head Completion: Surface Mount Well Vault
Well Development: Inertial water removal, lower water level and monitored recovery
Static Water Level before Development (TOC): 25.27 ft.

Split Spoon/Cored Intervals (ft) (bls.): 0-2, 5-7, 10-12,15-17, 20-22, 25-27, 30-32, 35-37, 38-40
Recovery respectively (Inches/ 2-ft): 18, 18, 18, 20, 24, 24, 24, 24, and 22

Lithological Description and Depth in feet Below Land Surface (bls.):

Depth (ft. bls.)	Description
0-2	Dry yellow brown silt w/ roots
3-5	Coarse sand and gravel
5-7	Light brown silt with gravel lenses
7-8	Coarse gravel
10-12	Light brown silt and clay some caliche, blocky
15-17	Light brown silt with roots: light brown silt, sand, gravel
20-22	Yellow brown fine sand with minor amts. of clay grades to gravel
25-27	Gravel grading to tight light brown clay
30-32	Soft light brown silty clay, minor gravel
35-37	Light brown wet fine sand with gravel lenses grading to light grey fine sand
38-40	Brown fine sand with coarse sand and gravel lenses at 39 ft. muddy sediments
40	TD

Observation Well - SV6

Well Location: NAD 27 – N39.04323, W114.48219
Tower Location: NAD 27 – N39.04306, W114.48251
Elevation: 5754 ft.
Drilled Depth: 30 feet bls.
Borehole Diameter: Augers 7.25-inch
Casing and Screen Size and Material, Wall Schedule, Joint Connection:
                 2-inch PVC, Schedule 40, Flush Joint
Screen Length/Slot Size: Nominal 15 feet/20 slots
Screen Interval from Top of Casing (TOC) – 14.79 ft. to 28.96 ft. w/ 6-inch well point
TOC = grade
Gravel Pack Interval (bls.): 13 ft. to 30 ft.
Bentonite Hole Plug Interval (hydrated) (bls.): 9 ft. to 13 ft.
Neat Cement Grout Interval (bls.): 0 to 9 ft.
Well Head Completion: Surface Mount Well Vault
Well Development: Inertial water removal, pumped at 2 gpm
Static Water Level before Development (TOC): 17.68 ft.

Split Spoon/Cored Intervals (ft bls.): 0-2, 5-7, 10-12, 15-17, 20-22, 25-27, 28-30
Recovery respectively (Inches/ 2-ft): 17, 20, 23, 24, 24, 20, and 13

Lithological Description and Depth in feet Below Land Surface (bls.):

Depth (ft. bls.)	Description
0-2	Soft light brown sand and silt grading to dry friable silt and clay
5-7	Hard orange red silty clay with roots (moist)
10-12	Brown friable silt, Fe stain roots
13-14	Reddish brown clay
15-17	Light reddish brown sand lenses with $CaCO_3$ concretions grades to massive reddish brown silty clay
20-22	Reddish brown silty clay, blocky
25-26	Light brown coarse sand and gravel
26-27	Moist clayey silt no structures
28-30	Reddish brown fine sand with some clay, high clay content in upper half of core
30	TD

Observation Well - SV7

Well Location: NAD 27 - N 39.34177, W 114.37028
Tower Location: NAD 27 - N 39.34173, W 114.37029
Elevation: 5539 ft.
Drilled Depth: 33.5 feet bls.
Borehole Diameter: Augers 7.25-inch
Casing and Screen Size and Material, Wall Schedule, Joint Connection:
                    2-inch PVC, Schedule 40, Flush Joint
Screen Length/Slot Size: Nominal 15 feet/20 slot
Screen Interval from Top of Casing (TOC) – 18 ft. to 32.25 ft. w/ 6-inch well point
TOC = grade
Gravel Pack Interval (bls.): 16 ft. to 33.5 ft.
Bentonite Hole Plug Interval (hydrated) (bls.): 13 ft. to 16 ft.
Neat Cement Grout Interval (bls.): 0 ft. to 13 ft.
Well Head Completion: Surface Mount Well Vault
Well Development: Inertial water removal, lower water level and monitored recovery
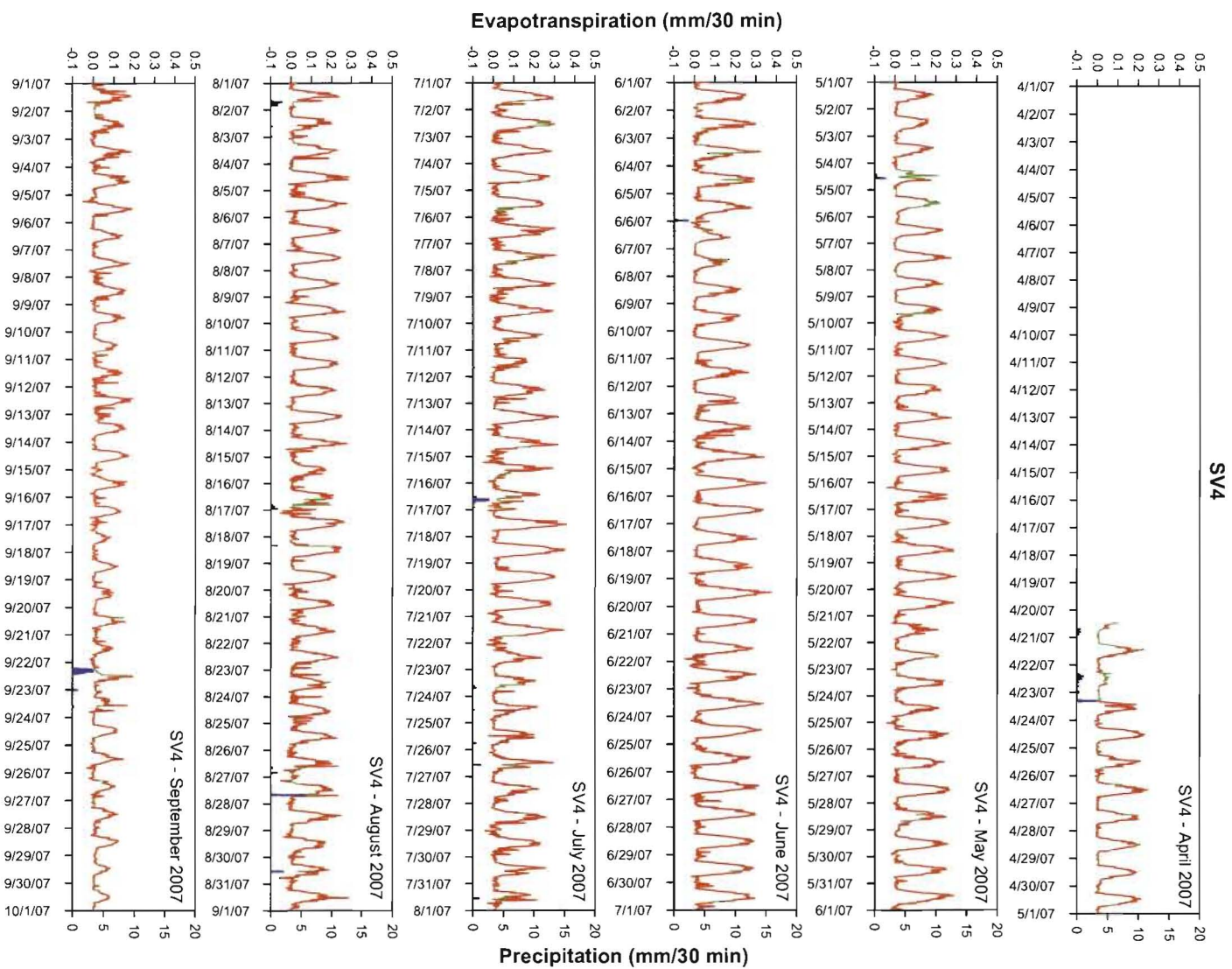Static Water Level before Development (TOC): 16.62 ft.

Split Spoon/Cored Intervals (ft bls.): 0-2, 5-7, 10-12, 15-17, 20-22, 25-27, 30-32
Recovery respectively (Inches/ 2-ft): 11, 22, 20, 22, 24, 24, and 24

Lithological Description and Depth in feet Below Land Surface (bls.):

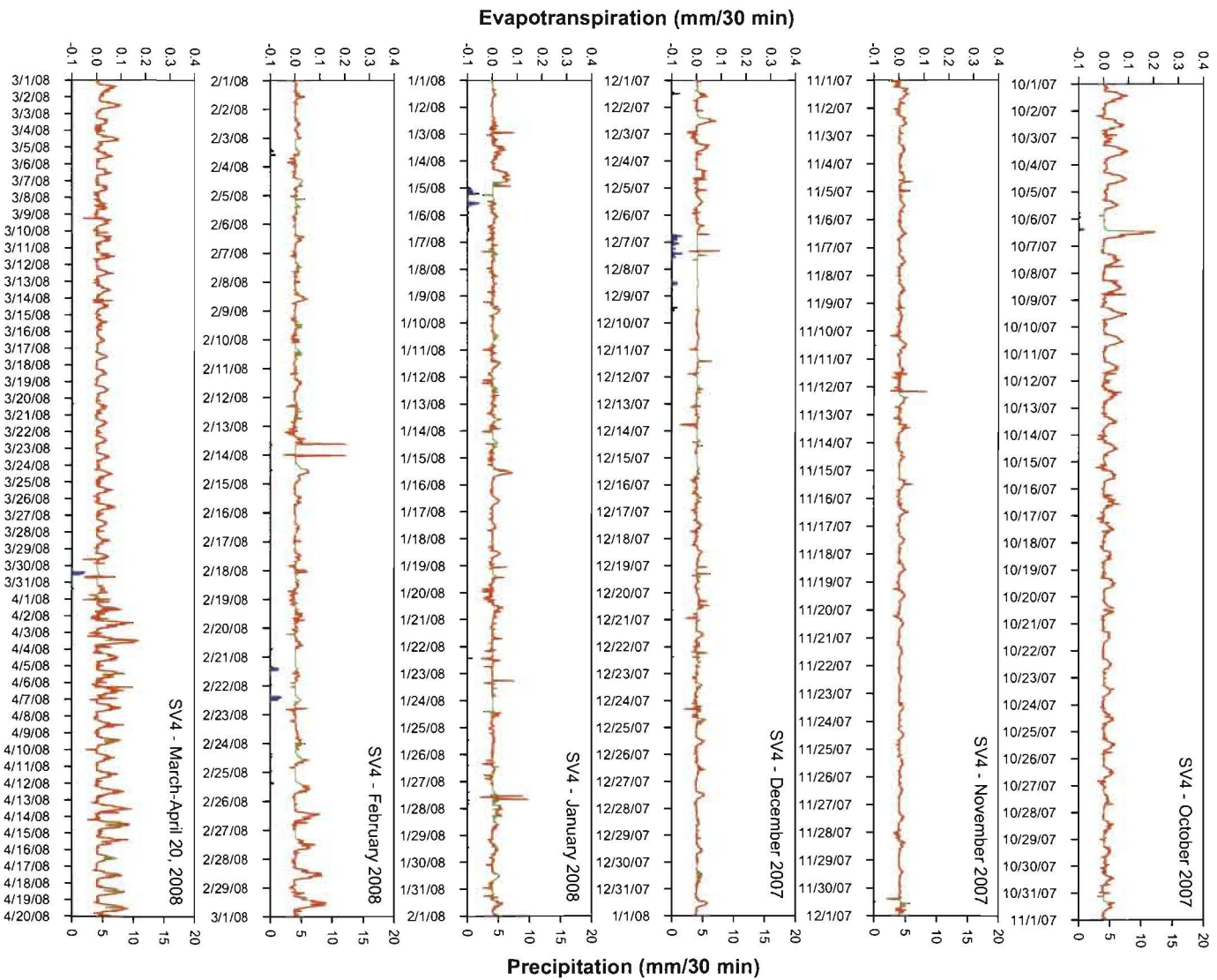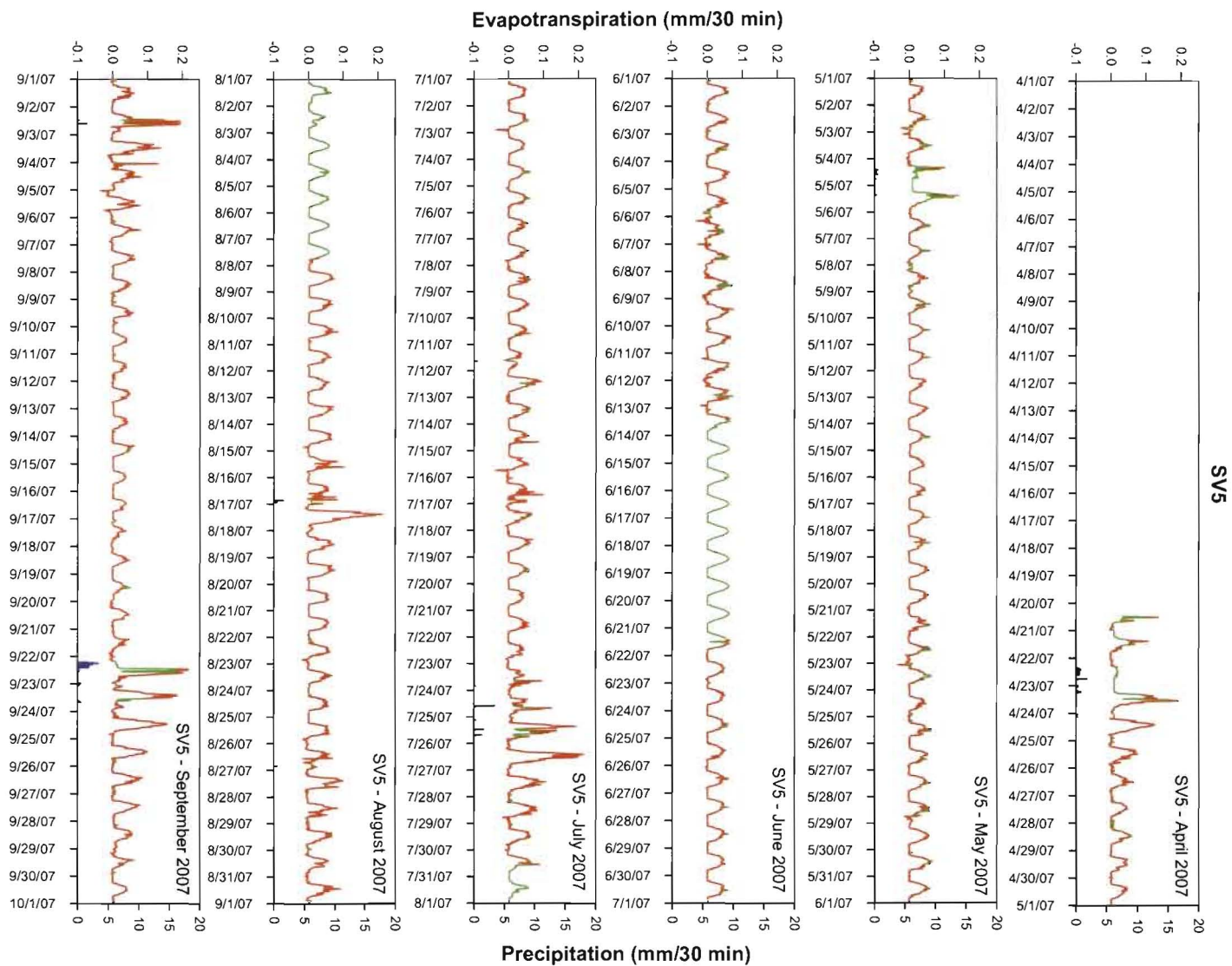| Depth (ft. bls.)	Description
0-2	Light brown sand and silt, roots
3-4	Light grey-green clay
5-7	Light greenish grey clay, massive no structures
10-12	Light brown silty clay transition to light greenish grey
15-17	Light greenish grey silty clay, roots, very moist
20-22	Light grey clay, v. moist, blocky, minor silt
25-27	Grey silty clay, roots, no structures: grades to higher silt
content	
30-32	Same as above
33.5	TD

Evapotranspiration (mm/30 min)

SV4

SV4 - April 2007

SV4 - May 2007

SV4 - June 2007

SV4 - July 2007

SV4 - August 2007

SV4 - September 2007

Precipitation (mm/30 min)

Figure B. Diel time course of ET (total mm per 30 minute) for each day and month from April 2007 to April 2008 for site SV4. Red points indicate measured ET values. Green points indicate calculated values using gap-filling regression equations (see Methods). Blue bars depict 30-minute total precipitation values in mm.
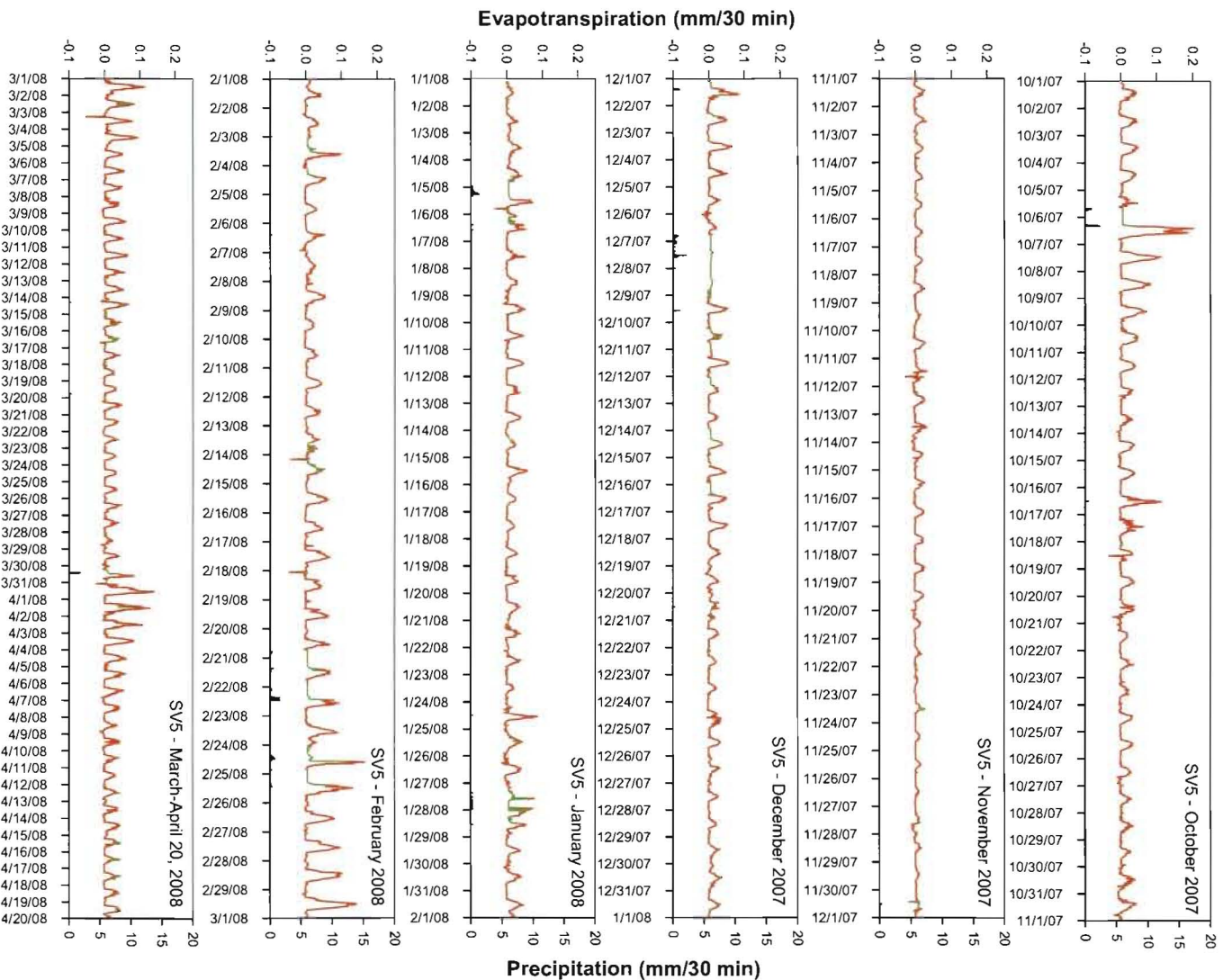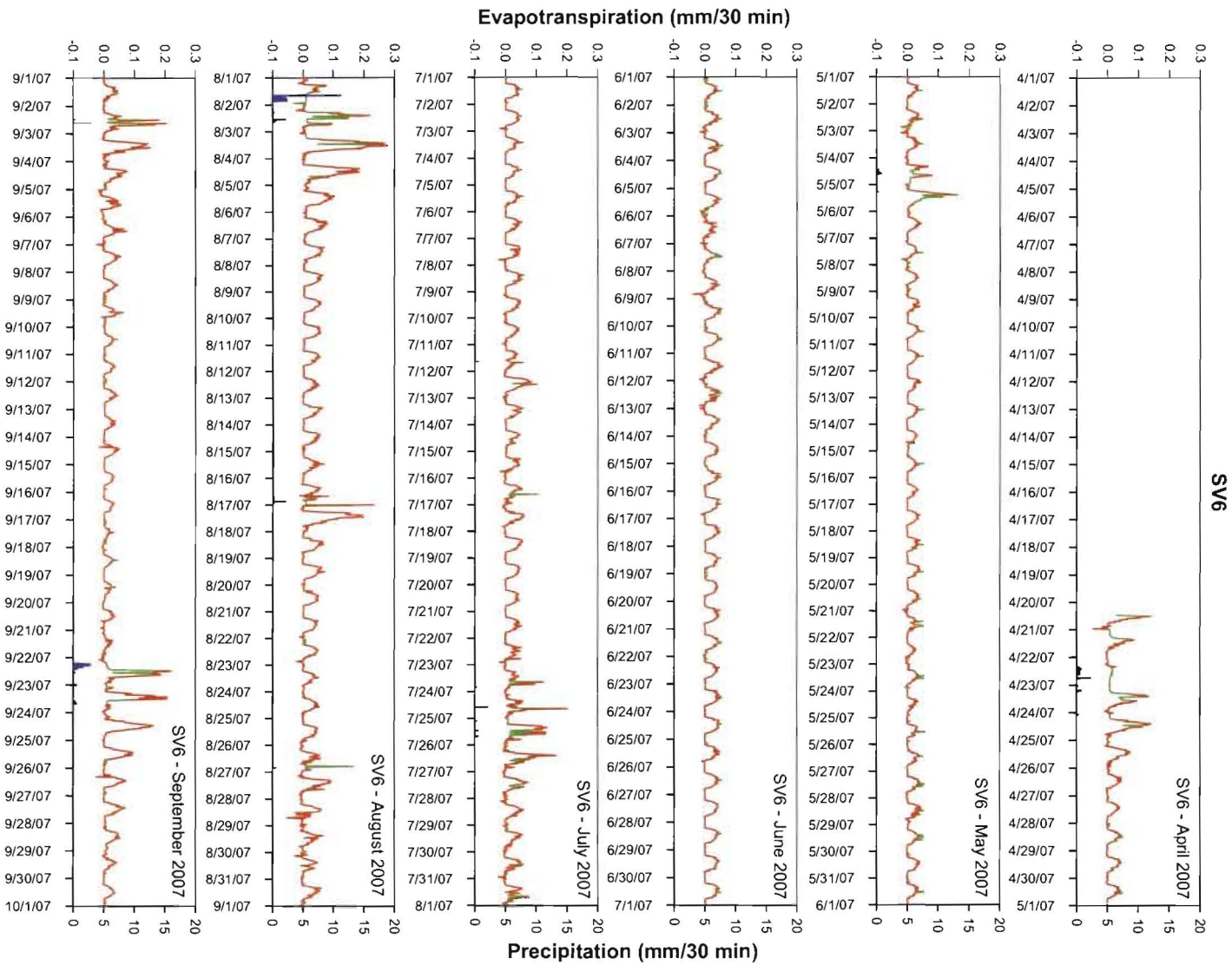
Evapotranspiration (mm/30 min)

SV5

SV5 - April 2007

SV5 - May 2007

SV5 - June 2007

SV5 - July 2007

SV5 - August 2007

SV5 - September 2007

Precipitation (mm/30 min)

Figure C. Diel time course of ET (total mm per 30 minute) for each day and month from April 2007 to April 2008 for site SV5. Red points indicate measured ET values. Green points indicate calculated values using gap-filling regression equations (see Methods). Blue bars depict 30-minute total precipitation values in mm.
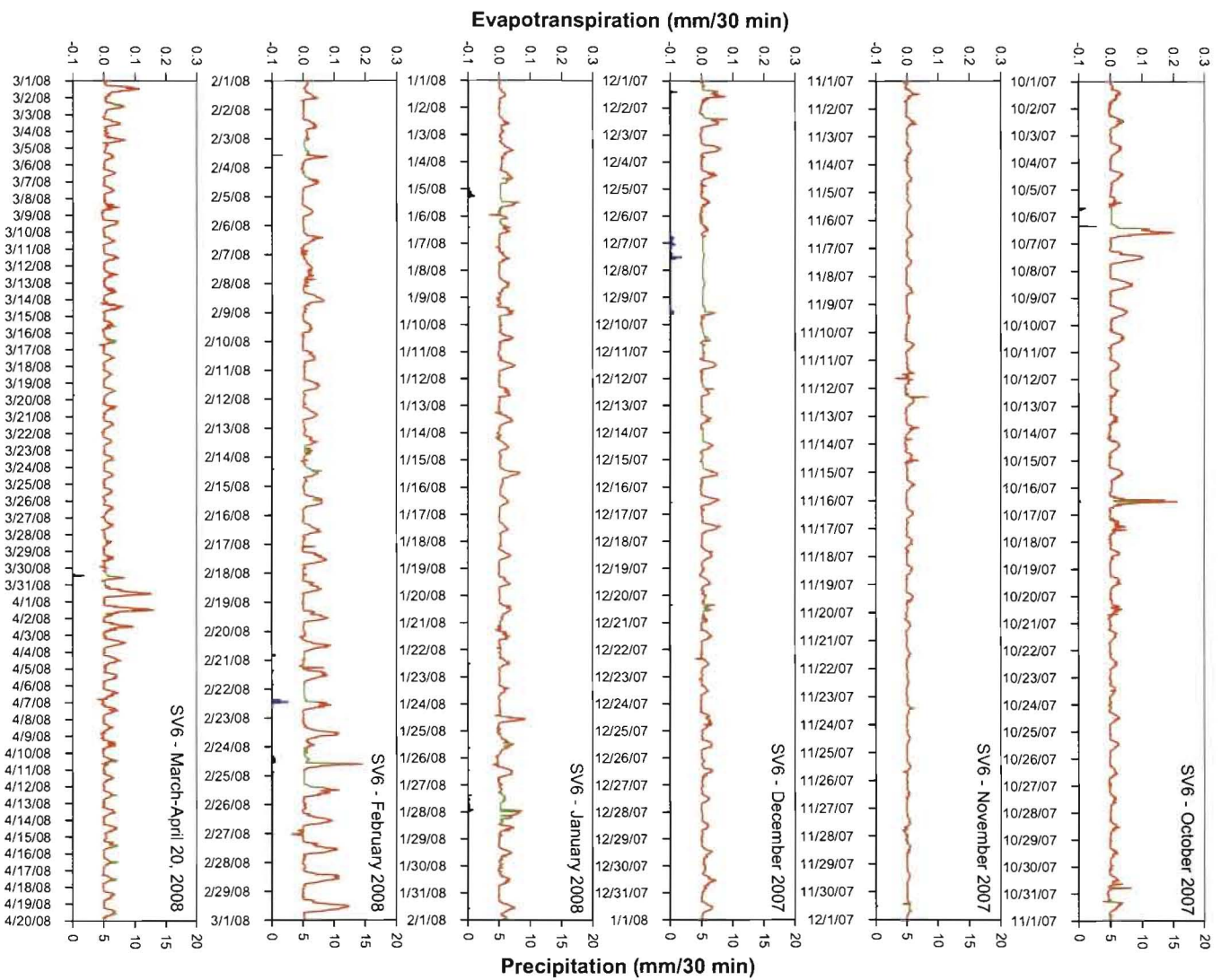
SV6

Evapotranspiration (mm/30 min)

Precipitation (mm/30 min)

SV6 - April 2007

SV6 - May 2007

SV6 - June 2007

SV6 - July 2007

SV6 - August 2007

SV6 - September 2007

Figure D. Diel time course of ET (total mm per 30 minute) for each day and month from April 2007 to April 2008 for site SV6. Red points indicate measured ET values. Green points indicate calculated values using gap-filling regression equations (see Methods). Blue bars indicate calculated values using gap-filling regression equations (see Methods).
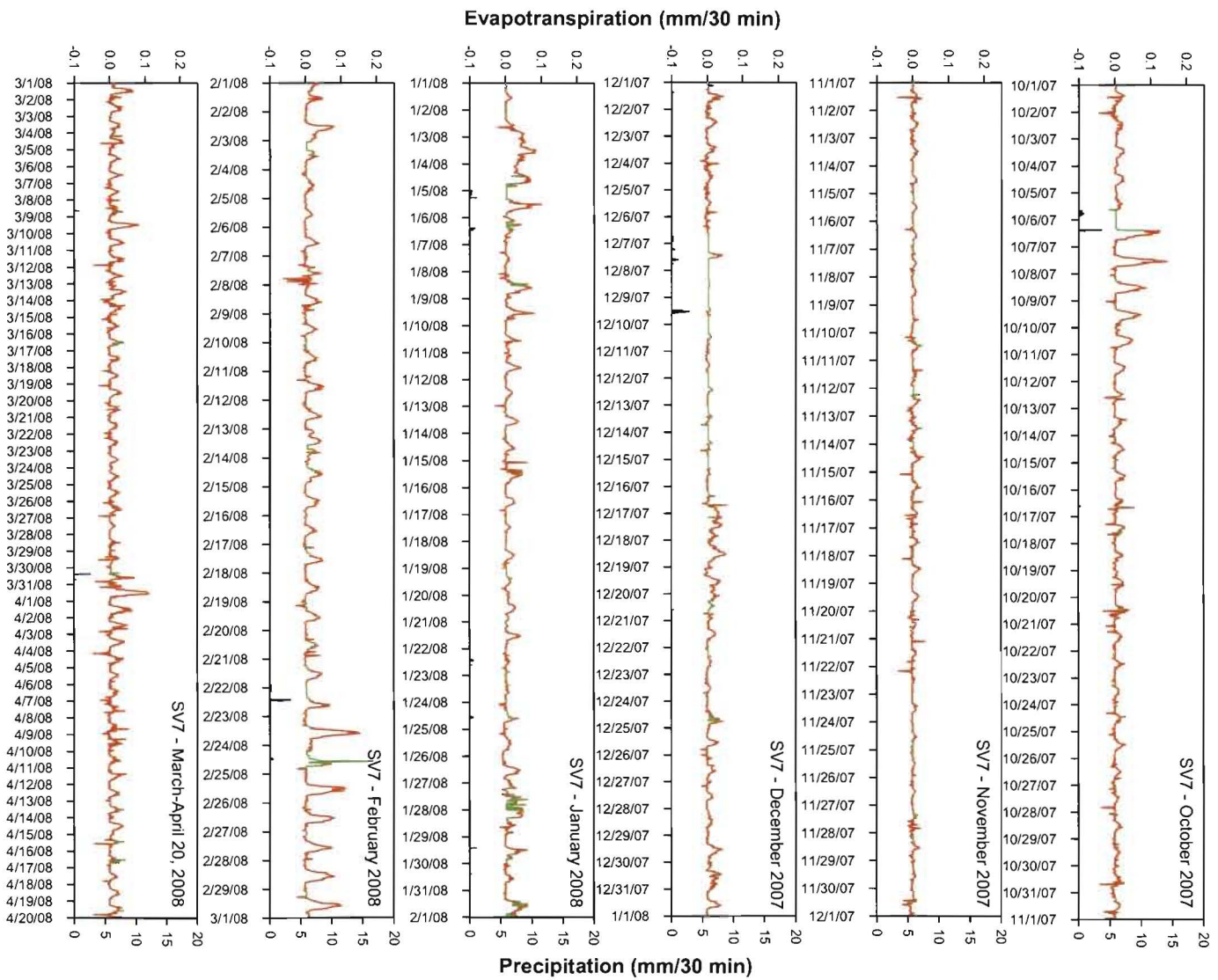
SV7
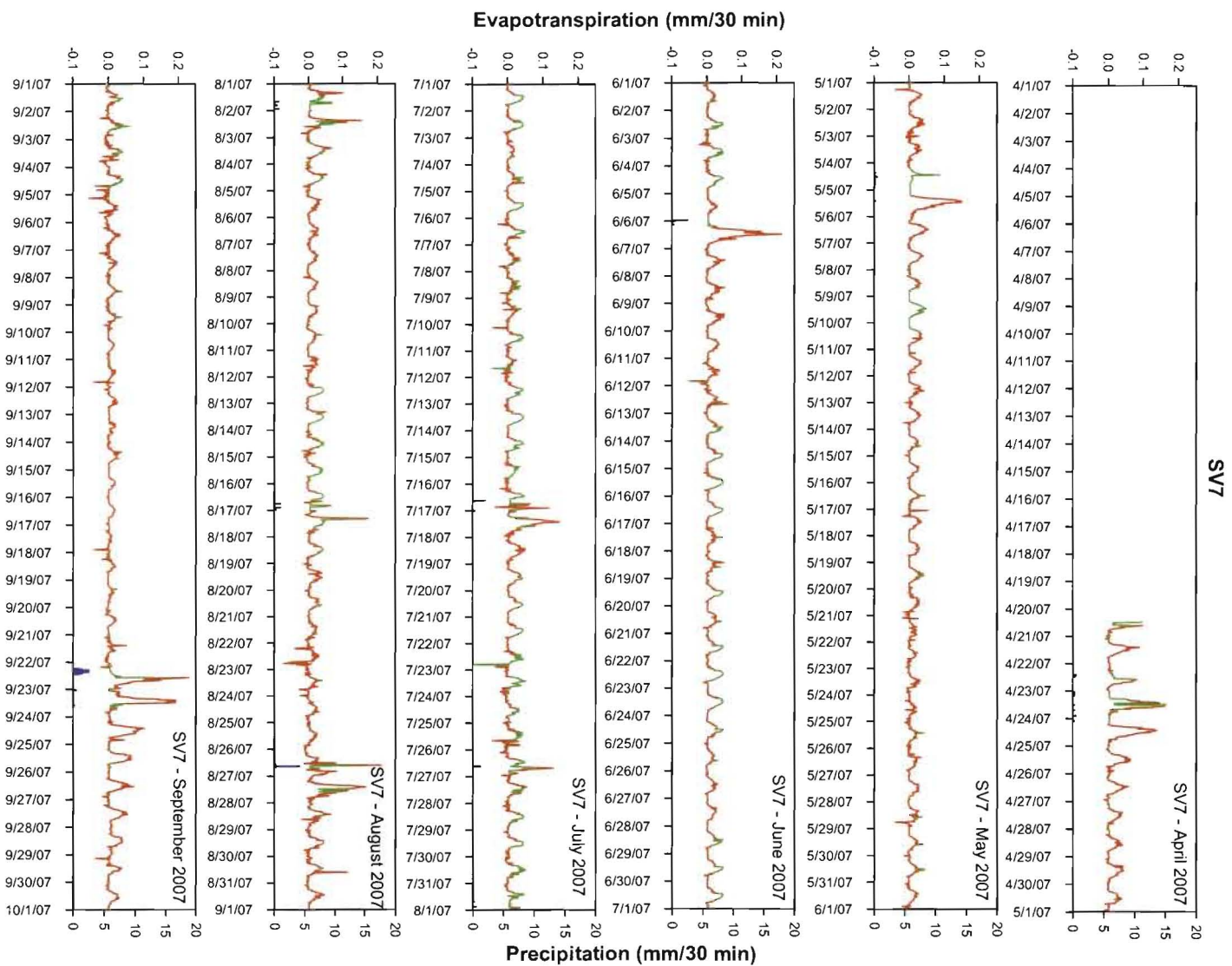
Figure E. Diel time course of ET (total mm per 30 minute) for each day and month from April 2007 to April 2008 for site SV7. Red points indicate measured ET values. Green points indicate calculated values using gap-filling regression equations (see Methods). Blue bars depict 30-minute total precipitation values in mm.